

1 Improvements in the integration of remote sensing and rock slope 2 modelling

3
4 Mirko Francioni (a), Riccardo Salvini (b), Doug Stead (c), John Coggan (a)

5 a) Camborne School of Mines, University of Exeter, Penryn, Cornwall, UK.

6 b) Department of Environment, Earth and Physical Sciences and Centre of Geotechnologies, University of Siena,
7 San Giovanni Valdarno, AR, Italy

8 c) Department of Earth Sciences, Simon Fraser University, Burnaby, BC, Canada

9
10 Key words:

11 Remote sensing, UAV, LiDAR, Slope stability analysis, Conventional and numerical modelling

12 **Abstract**

13 Over the last two decades the approach to the investigation of landslides has changed dramatically. The
14 advent of new technologies for engineering geological surveys and slope analyses has led to step-change
15 increases in the quality of data available for landslide studies. However, the use of such technologies in
16 the survey and analysis of slopes is often complex and may not always be either desirable or feasible. In
17 this context, this paper aims to improve the understanding of the use of remote sensing techniques for
18 rock mass characterization and provide guidance on how and when the data obtained from these
19 techniques can be used as input for stability analyses. Advantages and limitations of available digital
20 photogrammetry and laser scanning techniques will also be discussed in relation to their cost and the
21 quality of data that can be obtained. A critique of recent research data obtained from remote sensing
22 techniques is presented together with a discussion on use of the data for slope stability analysis. This
23 highlights how data use may be optimized to reduce both parameter and model uncertainty in future slope
24 analyses.

25 **1 Introduction**

26 The use of remote sensing techniques allows acquisition of detailed information on both the slope and
27 discontinuity geometry for study of landslide susceptibility and potential rock slope instability
28 mechanisms. Several authors have discussed the use of Digital Photogrammetry (DP) and Laser Scanning
29 (LS) in the study of natural and engineered slopes (Ghirotti and Genevois, 2007; Coggan et al., 2007;
30 Lato et al., 2009; Sturzenegger and Stead, 2009a, 2009b; Salvini et al., 2013; Francioni et al., 2014 and
31 2015, Spreafico et al., 2015). These techniques allow the acquisition of very detailed information on the
32 structural setting and slope geometry, particularly important in the case of steep inaccessible slopes. This
33 data can provide very useful input parameters for stability analyses, especially when considering the wide
34 range of software now available for both conventional and numerical methods of slope analyses (Stead
35 and Coggan, 2012; Stead and Wolter, 2015).

36 The principal aim of our research is to show the use of remote sensing techniques for providing the
37 necessary data for the varied methods of slope analysis. Long and short-range terrestrial laser scanning
38 and four approaches to photogrammetric survey will be presented, i.e. tripod, aerostatic balloon,
39 helicopter and Unmanned Aerial Vehicle (UAV) or drones. The data obtained from these different survey

40 techniques can be used in conventional (kinematic, limit equilibrium and rockfall) and more sophisticated
41 numerical (continuum, discontinuum and hybrid and rockfall run out) methods of analysis. The potential
42 use of other forms of remote sensing in slope investigations including airborne and mobile laser scanning,
43 aircraft photogrammetry, thermal and hyperspectral imaging and full waveform analysis will also be
44 briefly addressed.

45 Among conventional methods, kinematic analysis remains the simplest method to study rock slope
46 stability and can be extremely useful in preliminary assessment of potential instability mechanisms.
47 Results from this analysis are strictly related to the geometric orientation of discontinuity surfaces relative
48 to the slope. It is important that structural domains be identified and that the measured discontinuity
49 parameters representative of the area be assessed. In this context DP and LS are ideally suited to collect
50 input data that is more representative of the study area, which may often be inaccessible to conventional
51 methods of discontinuity data collection. As part of the analysis it is essential that the variation in
52 discontinuity sets and their orientation within a slope be assessed and the effect of structural geology on
53 slope stability be fully considered. The use of remote sensing methods allows such spatial variations in
54 structure (with slope height and along the slope) to be investigated more comprehensively and efficiently.
55 Francioni et al. (2015) showed how interpolation of remotely sensed data using GIS techniques can be
56 used to perform a more rigorous deterministic kinematic analysis of slopes.

57 When using limit equilibrium methods the geometry of discontinuities and slopes is considered together
58 with force and/or moment equilibrium conditions. DP and LS data can be integrated with conventional
59 engineering geological surveys and used for deterministic and probabilistic stability analysis. The
60 geometry of the rock blocks and the discontinuities obtained from remote sensing techniques and the
61 physical characteristics of discontinuities and rock mass from both engineering geological survey and
62 close range LS/photogrammetry can be used to calculate the Factor of Safety of the blocks within the
63 slope (Salvini et al. 2011, 2013). Conventional limit equilibrium slope stability analysis can also be
64 supplemented by rockfall calculations for risk and hazard assessments. This is particularly important for
65 the definition of areas that can be affected by potential rockfall and for the subsequent creation of hazard
66 maps (maps highlighting area of potential instability and/or rockfall). DP and LS can play a key role in
67 defining the geometry and topography of the slope and the land cover which are all essential input data in
68 rockfall run out simulation.

69 Numerical modelling has been increasingly used in recent years for stability analyses (Brideau and Stead,
70 2010; Brideau et al., 2011; Stead and Coggan, 2012; Francioni et al., 2014 and 2015; Stead and Wolter,
71 2015 and Spreafico et al., 2015 and 2017). The reliability of a numerical model is however connected to
72 the quality of input data and the assumed constitutive models and failure mode. DP and LS can greatly
73 improve the quantity and quality of the available data for slope analysis and can also be used, where
74 appropriate, to create sophisticated stochastic Discrete Fracture Networks (DFN) for incorporation into
75 numerical models.

76 2 Remote sensing sensors

77 2.1 Digital Photogrammetry

78 In the last two decades, the availability of new survey techniques and software processing tools has
79 resulted in a marked increase in the use of DP.

80 Conventional acquisition methods include independent convergent, image fan and image strip models
81 (Figure 1A-C). These methods are explained in detail by Birch (2006) and their application discussed by
82 Sturzenegger and Stead (2009a, 2009b); the choice of method being decided according to site specific
83 slope conditions. Figure 1A shows the independent convergent model; the advantage of this method is
84 that almost 100% of the images are used to build the model and if multiple models are required to cover
85 the slope, very little overlap is required between models. Figure 1B shows the image fan method; this is
86 similar to the independent method with the exception that the images are captured from specific camera
87 locations (which are not independent). In this way, there are fewer unknowns to be determined (since the
88 camera positions are the same) and the precision of the models is greater; this can be used also with high
89 focal length lenses for long range photogrammetry (Sturzenegger and Stead, 2009a, 2009b; Birch, 2006).
90 The last method is the image strip setup (Figure 1C) where a series of parallel images with a typical 60%
91 overlap is required. The high degree of overlap between images results in precise orientation of the
92 model, significantly reducing the number of control points required. This method, in addition to being
93 suitable for aerial photogrammetry, is also used in terrestrial photogrammetry when the stations and the
94 outcrop are not very far apart (as the distance becomes larger, depth accuracy is reduced) and the slope is
95 not very high. A typical example of the use of this method is in the survey of underground tunnels when
96 the distance between the camera and the rock wall is small and the acquisition of a series of parallel
97 images is the easiest way to proceed.

98 The coordinates of the camera location or the coordinates of ground control points located in the surveyed
99 area are required to scale/geo-reference the photogrammetric models. In recent years the use of Structure
100 from Motion (SfM) imaging techniques (and software) has increased significantly making the routine use
101 of photogrammetry in engineering practice easier and even more attractive. Although SfM still requires
102 the use of ground control points to scale/geo-reference the model, the creation of the 3D model is much
103 easier and faster. This is due to a highly redundant bundle adjustment based on matching features in
104 multiple overlapping photographs (Figure 1D). An introduction to this technique is given by Westoby et
105 al. (2012) while applications of SfM techniques in engineering practice have been recently presented by
106 Lucieer et al. (2014) and Salvini et al. (2016).

107 Another type of acquisition technique is the use of stereo cameras rigidly mounted that allow the
108 acquisition of photographs from two cameras with a known baseline (distance between the cameras)
109 (Firpo et al., 2011; Francioni et al., 2014). In such cases the baseline is known and if the camera is
110 calibrated, it is possible to reconstruct a scaled 3D photogrammetric model.

111 2.2 Laser Scanning

112 LS allows the remote acquisition of information from an observed object including both morphological
113 characteristics (altitude, spatial coordinates, etc.) and physical properties, e.g. the intensity of the reflected
114 signal that can be correlated to the object material, temperature, humidity, etc.

115 LS can also involve both short and long range acquisition. Long-range laser scanners (up to 6 km) are
116 particularly useful for wide and high rock slopes. It is possible to set up the laser scanner at a considerable
117 distance from the slope, hence decreasing the number of occlusions when working with very elevated
118 slopes. Moreover, because of accessibility issues, sometimes it is not possible to set up the instrument
119 close to the slope, and without a long-range laser scanner, the acquisition would not be possible. The
120 recent use of long range LS for landslide analysis is documented by Barbarella et al. (2015).

121 Short range laser scanners are fast and very precise with a wide vertical field of view and for these
122 reasons have mostly been used in engineering geology in underground mining and for small rock slopes,
123 where the instrument can (or has to) be set close to the slope (Francioni et al., 2013 and 2014).

124 Time-of-flight and phase difference are the two types of measurement principles by which laser scanners
125 obtain geometric and physical data. An introduction to these techniques, and laser scanner specifications,
126 are highlighted by Beraldin (2004) and Fröhlich and Mettenleiter (2004). Time-of-flight has been the
127 most used measurement technique to date; it allows for measuring the geometry and the reflectivity of an
128 object from a few meters to kilometers in distance. The newly available phase difference measurement
129 terrestrial laser scanners (full waveform LS) have seen considerable research in the last few years. With
130 this technology it is possible to capture additional metrics of the rock slope surface, which allow
131 significantly reduced uncertainties in change detection (Afana et al., 2013). Using this approach,
132 geometric and radiometric target surface information can be obtained and, at the same time, retain the
133 spatially rich detailed point-clouds.

134 The advent of full waveform LS make the LS techniques more attractive but it has to be noted that the
135 cost of full waveform LiDAR technology is currently significantly higher than time-of-flight instruments
136 and DP.

137 3 Remote sensing platforms

138 3.1 Ground based platforms

139 Ground based remote sensing instrument platforms such as tripods, hand-held devices and vehicles are
140 commonly used in engineering geology. Although these systems are simple to use and cost effective, they
141 have significant limitations related to the slope elevation; when a survey has to be conducted at the
142 bottom of a high slope, occlusions can seriously compromise the final model (Lato et al., 2009; Francioni
143 et al., 2014). Sturzenegger and Stead (2009a, 2009b) highlighted the importance of understanding
144 possible bias related to the use of this technique and how the results can be affected by occlusions.
145 Nevertheless, this method has been successfully used by several authors in the analysis of rock slopes

146 (Haneberg et al., 2006; Bonilla-Sierra et al., 2015; Havaej et al., 2016). In the following sections, the most
147 common types of platform for slope surveys are presented.

148 *3.1.1 Ground based Digital Photogrammetry with hand-held camera or tripod*

149 A hand-held camera or tripod are the simplest and most convenient photogrammetric survey methods.
150 The use of a tripod results in acquisition of high quality photographs and reduces the distortions related to
151 camera vibrations. Another advantage of the use of a tripod is the possibility to perform long range
152 photogrammetry (Sturzenegger and Stead, 2009a; 2009b). It is also possible to use a tripod together with
153 a reamed bar in order to maintain a constant line of sight and to precisely control the distance between
154 sequential photographs (Salvini and Francioni, 2013). Figure 2A-B shows the application of this
155 technique with and without a reamed bar respectively in two case studies, a rock outcrop along the ‘Sea to
156 Sky Highway’ in British Columbia, Canada and in a Carrara marble quarry, Italy.

157 A GigaPan (GigaPan, 2016) robotic tripod may be used for both producing high resolution panoramas of
158 rock slopes or conventional acquisition of images for photogrammetry.

159 The use of hand-held camera survey technique has increased markedly with the advent of SfM techniques
160 as they overcome some of the limitations related to the position of the camera, and using a consistent
161 number of images it is possible obtain a detailed 3D model of the study area.

162 *3.1.2 Ground based Laser Scanning with tripod*

163 Ground based LS, or terrestrial LiDAR is a survey technique for rapidly obtaining high precision slope
164 geometry and deriving geological structure. One of the most difficult steps in using terrestrial LS is the
165 point cloud registration which allows for the integration of several point clouds into a unique reference
166 system (Francioni et al., 2014). Francioni et al. (2014) showed how this problem can be solved using an
167 integrated topographic system. Moreover, some of the most recent software for point cloud management
168 have built-in modules for the automatic registration of point clouds based on the recognition of common
169 points between different point clouds (ICP - Iterative Closest Point, Besl and Mckay, 1992).

170 Figure 3 shows two 3D representations of an outcrop located along the Sea to Sky Highway, BC, Canada
171 obtained using a tripod and a Riegl VZ4000 scanner (very long-range laser scanner with online waveform
172 processing; Riegl, 2014). Figure 3A shows the 3D model of the road cut visualized using the RGB
173 information gained from the internal digital camera of the laser scanner. Figure 3B shows the same
174 outcrop visualized as the wave amplitude (dB). The use of waveform analysis (in this case wave
175 amplitude) allows recognition and highlighting of different rock types. It is clearly shown that the
176 amplitude generated from the overlying basalt columns in the 3D model have a higher value compared to
177 the lower competent formation beneath. Using the same theory as applied in the airborne LiDAR, this
178 technology allows for recording different object echoes. Figure 4 shows the acquisition of the
179 photographs (Figure 4A), RGB point cloud (Figure 4B) and the visualization of the four echoes registered
180 by the Riegl VZ4000 laser scanner (Riegl, 2014) for a geological outcrop located along the ‘Sea to Sky
181 Highway’ (Figure 4C). This facility is important for filtering the point cloud based on the different
182 arrivals (first, last or single) and obtaining more information where there is vegetation or objects located
183 along the LiDAR line-of-sight.

184 **3.1.3 *Ground based mobile Laser Scanning***

185 Mobile LS refers to the use of LS from moving platforms. The common utilization of this technique is
186 through the use of wheeled vehicles (the instrument is usually mounted on the vehicle roof) for road or
187 scene mapping purposes. However, mobile laser scanning systems are not restricted to wheeled vehicles
188 as they can be mounted on any moving platforms, such as trains and boats. The main advantage of this
189 technique is the speed with which it is possible to survey entire streets or buildings. Moreover, in case of
190 coastlines, the use of a boat can allow scanning of cliff faces from the sea. Since the LS data are acquired
191 from a moving platform, georeferencing the data can be more complicated. For this reason, when using
192 this type of platform LS instruments are supplemented by GPS and an Inertial Measurement Unit (IMU).

193 The use of mobile LS in engineering geology and especially in the study of landslides has been presented
194 by Michoud et al. (2015) who describe an interesting case study in High Normandy, France. They tested
195 boat-based LS capabilities by scanning 3D point clouds of unstable coastal cliffs showing the potential
196 use of boat-based LS to detect rockfalls and erosional deposits including multi-temporal acquisitions, to
197 monitor large slope changes.

198 New generation LS are very flexible and can be also hand-held or used on platforms such as backpacks
199 thereby providing the ability to map areas while walking geological traverses.

200 Hand-held and backpack LS has to date not been widely used in the study of rock slopes but has seen a
201 wide range of general applications including heritage site mapping, crime scene investigations and civil
202 engineering projects. In engineering geology, the most important application to date is related to
203 underground tunnel surveys (Eyre et al., 2016). Hand-held LS has the advantage of being very rapid and
204 easy to use but currently results in less precision and resolution than traditional LS. It has limited range,
205 making it ideal for tunnelling applications, but less applicable to slope and landslide analysis that require
206 greater distance.

207 **3.2 Airborne platforms**

208 Airplane, satellite, aerostatic balloon, helicopter and UAV are the most common airborne platforms
209 currently available. Due to the high spatial resolution achievable with the new digital aerial photo-
210 cameras and LS devices, airplane and satellite data can be used in the photo-interpretation of geotechnical
211 projects at a large scale. However, despite the high quality of photographs and point clouds, the point of
212 observation at the nadir is sub-optimal in the study of natural and artificial rock slopes characterised by
213 very steep or even vertical slope sections. This problem can be overcome using platforms that allow
214 change of the point of observation such as an aerostatic balloon, helicopter or UAV. This also
215 significantly reduces most of the occlusion problems highlighted for the ground based platforms.

216 **3.2.1 *Airborne Digital Photogrammetry using aerial or satellite imagery***

217 Aerial photogrammetry refers to imaging acquired through aerial or satellite platforms. In airplane and
218 satellite photogrammetry the camera is usually pointed vertically towards the ground. Multiple
219 overlapping photographs of the ground are taken as the aircraft/satellite flies along a flight path. These
220 photographs are processed either using a stereo-plotter or in automated processing for Digital Elevation

221 Model and orthophoto creation. These techniques are therefore used in numerous types of cartographic
222 application, from military and regional small-scale maps, to that of medium- and large-scale technical
223 maps (topographic, geological, geomorphological, land use, etc.). Airplane/satellite photogrammetry is
224 very useful in regional engineering-geological mapping and for detecting landslide related geomorphic
225 landforms (Wolter et al., 2016; Mantovani et al., 2016, Clayton et al., 2017. Donati et al., 2017).

226 3.2.2 Airborne Digital Photogrammetry using an aerostatic balloon

227 Of the platforms presented, the use of the aerostatic balloon has been far less common in engineering
228 geology. DP with an aerostatic balloon can be carried with one single camera (Take et al., 2007) or stereo
229 pairs (Firpo, 2011, Francioni, 2014). Firpo et al. (2011) and Francioni et al. (2014) show the use of an
230 aerostatic helium-filled balloon carrying an apparatus that consists of an aluminum bar with two camera
231 slots for the study of high steep quarry slopes in Carrara (Italy) (Figure 5A, B and C). The geometry and
232 length of the apparatus can vary depending on the baseline that is used and more camera slots for a video
233 camera may be added to capture in real time the slope face during image acquisition (Figure 5B, C)
234 (Firpo, 2011; Francioni, 2014). Four electrical winches are used to drive the balloon (Figure 5D) while
235 image acquisition is controlled by a PC-driven radio system which guarantees synchronous data
236 acquisition (Firpo 2011, Francioni 2014). In this way, stereo-pairs can be acquired simultaneously and
237 used to build a scaled photogrammetric model using the image strip (the baseline being perfectly known
238 by using the frame) or independent convergent models. Francioni et al. (2014) describe the use of an
239 aerostatic balloon in a complex slope in the Apuan Alps showing the possible use of this technique and
240 highlighting some of the complex procedures involved. Balloon used to date for photogrammetric
241 purposes can reach up to 300 m from the ground (Firpo e al., 2011; Francioni 2014). However, the area to
242 be imaged must be accessible and sufficiently wide (Francioni et al., 2014). Weather conditions can also
243 be a major limitation in the use of this method, which is best conducted in the absence of rain and,
244 especially, wind.

245 3.2.3 Airborne Digital Photogrammetry using a helicopter

246 The aerostatic balloon can be used only if appropriate site and weather conditions persist and a suitable
247 inexpensive source of helium gas is available. When these conditions are not present or in the case of
248 slopes higher than 300 meters this technique cannot be utilized. In such cases, helicopters can provide an
249 ideal data acquisition platform. The photogrammetric equipment described in Salvini et al., 2011 and
250 Salvini et al., 2013, consist of an aluminium or steel frame adapted to fit a helicopter landing skid
251 supporting two digital cameras and two GPS antennas at its extremities. The equipment is connected and
252 controlled in real time from operators in the helicopter. In this way, it is also possible to use Differential
253 GPS (the power source being located in the helicopter) which helps to know the position of the camera
254 and the orientation of the frame at the moment of the image acquisition. In this case, stereo pairs are also
255 acquired simultaneously and used to build a scaled photogrammetric model through image strip or
256 independent convergent models. Occlusions can be considerably reduced with a careful work plan as it is
257 possible to check the photograph acquisition in real time from the helicopter. Figure 6 shows the
258 photogrammetric equipment developed by Salvini et al. (2013) and utilized in the analysis of a rock slope
259 sited in Northern Italy.

260 Recent research has seen an increasing use of hand-held cameras in helicopter platforms to obtain high
261 quality SfM models (Gauthier et al., 2015). Digital SLR cameras now contain in-built GPS or
262 conveniently mounted GPS adaptors. The use of hand-held cameras in the helicopter is well demonstrated
263 by Vallet et al. (2000), Copons and Vilaplana (2008), Gauthier et al. (2015).

264 Helicopter platforms for DP have two main limitations, the first being the high costs involved and the
265 second the difficulty in maintaining the stability and direction of the aircraft throughout the
266 photogrammetric survey. Subsequently, this can create problems for the orientation of the photographs.
267 However, with the acquisition of a considerable number of images, use of topographic survey to define
268 the coordinates of Ground Control Points and SfM software, this problem can be mitigated.

269 *3.2.4 Airborne Digital Photogrammetry using an UAV*

270 UAV systems are now routinely used in a wide variety of engineering and geoscience fields and include
271 both fixed wing and multi-rotor options. UAV systems are highly flexible and provide an ideal platform
272 for the acquisition of high resolution photographic images along pre-programmed flight lines/paths. They
273 overcome most of the limitations noted for the other platform providing increased spatial close range
274 coverage of inaccessible rock slope outcrops with reduced occlusions. Basically, the use of a UAV allows
275 acquisition of areas that could not be surveyed with any other vehicle or methodology. Moreover, remote
276 control of the UAV reduces the need for hire of a helicopter and operators, the cost of which may be
277 significant. This makes the UAV method less expensive than the aerostatic balloon or helicopter.

278 Although UAV-based photography is the most common and inexpensive technique used at present,
279 UAVs are increasingly being used to capture thermal, hyperspectral and Light Detection and Ranging
280 (LiDAR) imagery. An on-board GPS-IMU system provides the positions of the UAV camera at the
281 moment of image acquisition and independent convergent SfM methods are used to build the
282 photogrammetric model. Figure 7 shows a Falcon 8 UAV (Figure 7A) used during the survey of the
283 Lorano open pit in the Carrara marble district, Italy (Figure 7B) (Francioni et al., 2015).

284 The use of the UAV in the earth sciences and engineering geology is well-documented in the recent
285 literature (Haarbrink and Eisenbeiss, 2008; Niethammer et al., 2010; Francioni et al., 2015; Salvini et al.
286 2015a; Assali et al., 2016; Westin, 2017; Donati et al., 2017). The most important disadvantages in using
287 the UAV technique is that it can be used only in absence of wind/rain. This can present a major problem
288 where local wind eddies exist along high mountain slopes. In case of multi-rotor options it can also be
289 difficult to acquire photographs maintaining the same line-of-sight (Francioni et al., 2015) and this can
290 generate misalignment of photographs and major potential errors during their orientation. Obtaining a
291 large number of photographs and using SfM software can, however, reduce these errors and make the
292 UAV technique easier and more attractive. An additional current limitation in the use of the UAV that
293 especially affects multi-rotor systems is the often limited battery life which can require the UAV pilot be
294 within close range of the take-off/landing area. Where spatially extensive slopes require surveying,
295 multiple battery packs may be essential. The advent of inexpensive UAV systems represents the most
296 interesting and promising innovation regarding remote sensing techniques as it provides a very powerful
297 and flexible instrument for the acquisition of photographs (Colomina and Molina, 2014; Francioni et al.,
298 2015; Westin, 2017; Donati et al., 2017). Their use will, most likely, become more frequent in the coming
299 years, and it is important to continue studies on their utilization in the field of engineering geology,

300 particularly with respect to change detection/slope monitoring and multi-sensor capabilities. A potential
301 future disadvantage in the use of UAV technology is the increasing flight restrictions in their use due to
302 abuse of the technology from recreational use. In some countries, it may become increasingly difficult to
303 obtain approval for UAV flights.

304 3.2.5 Airborne LiDAR

305 Airborne LiDAR devices emit up to 150,000 pulses per second and a sensor measures the amount of time
306 it takes for each pulse to bounce back (or return). An IMU integrated with a differential kinematic GPS
307 provides information about the position and attitude of the sensor. Airborne LiDAR offers advantages
308 compared to traditional measurement systems such as the ability to penetrate vegetation cover, (first-last
309 pulse mode), the possibility to record data at night and over a large survey area. Aerial LiDAR is widely
310 utilised in engineering geology for landslide hazard mapping and modeling, change-detection, cliff
311 erosion, and rockfall runout (Jaboyedoff et al., 2012; Lato et al., 2016; Piacentini et al., 2015). The use of
312 this technique to detect geomorphic and major structural features for identifying palaeo-landslides has
313 been recently shown by Clague et al. (2015). Figure 8 provides an example of Airborne LiDAR and GIS
314 for highlighting landslide related geomorphic features at Mount Burnaby, British Columbia, Canada.

315 Recently, as a result of the full waveform systems, aerial LiDAR is also being utilized for the
316 characterization of surface material from the analysis of the physical backscattering measurements
317 (Sumnall et al., 2016).

318 3.2.6 Airborne LiDAR using an UAV

319 With advent of UAV solutions, small LS devices have been installed with the possibility to scan any type
320 of slope surface. This type of LS acquisition presents the same advantages and limitations discussed in
321 section 3.2.4 for DP with UAV. However, it be noted that accuracy, precision and resolution of this
322 technique are poorer than that obtained using ground based systems. This type of platform offers much
323 more flexibility and overcomes limitations related to occlusion and point of observation. The use of UAV
324 LS in engineering geology is not well documented to date but is an area of significant potential future
325 research.

326 **4 Remote sensing and rock slope stability analyses**

327 A remarkable quantity of data can be obtained through the use of terrestrial remote sensing techniques.
328 This information can be used for different types of slope analyses, varying from simple kinematic
329 admissibility tests, to more complex numerical simulations.

330 **4.1 Remote sensing and conventional methods of slope analysis**

331 Conventional methods of slope analysis can include kinematic analysis, limit equilibrium calculations and
332 run out analysis (Stead et al., 2006).

333 Kinematic analysis investigates the likelihood that unfavourably oriented discontinuities will generate
334 discontinuity-controlled instability such as planar, wedge or toppling slope failures. The kinematic test

335 considers the relative slope and discontinuity orientations and the effective friction angle along the
336 discontinuity surfaces to determine whether a block can potentially move or not. This type of analysis can
337 be carried out using a stereonet and/or 2D/3D vector analysis applied to 2D/3D rock structure models.
338 Although a very simple analysis it is a very useful preliminary tool allowing for a first estimation of
339 potential failure and identification of potential key blocks. Stead et al. (2006), Brideau et al (2011) and
340 Francioni et al. (2015) note that results of this analysis are influenced to a large degree by reliability of the
341 discontinuity survey and the accuracy of the slope topography. Recent developments in available
342 commercial software allow for including all the measured discontinuities in the rock slope analysis
343 (instead of just considering the mean joint set orientations obtained from joint surveys at the slope toe).
344 This makes the use of remote sensing techniques highly relevant because the data from remote sensing are
345 representative of the entire slope from the toe to the crest. Figure 9 highlights this concept showing a
346 comparison of two kinematic analyses that were performed with engineering geological (Figure 9A) and
347 remote sensing data (Figure 9B) in the Lorano open pit (Carrara, Italy) (Francioni et al., 2015). The
348 results clearly show the difference in the two data sets in relation to the different spatial areas covered by
349 the two surveys. The conventional engineering geological survey was performed only in accessible areas
350 while the remotely sensed data from DP covered the entire slope. Figure 10 shows a photograph of the
351 Lorano open pit (Figure 10A) and the 3D model obtained using UAV and SfM techniques (Figure 10B).

352 Recent developments in kinematic software allow highly interactive kinematic stability analysis of slopes
353 with semi-probabilistic methods of failure modes. The assigning of discontinuity attributes (roughness,
354 persistence, infill, spacing etc.) is also supported. Kinematic analysis of a slope should always consider
355 the measured spatial location of major structures as determined using remote sensing; this practice,
356 combined with the use of structural domains, avoids the identification of “fictitious” failure modes
357 indicated on a stereonet but not observed in the slope face. It is emphasized that wherever possible remote
358 sensing methods should be supplemented with field mapping and the use of photographic site
359 observations. Oppikofer (2009), Brideau et al. (2011) and Francioni et al. (2015) showed that remote
360 sensing and kinematic analysis can be usefully integrated with Geographic Information Systems (GIS) for
361 developing thematic maps. These thematic maps can clearly illustrate how the results of a kinematic slope
362 failure analysis can change with location in the slope, depending on the topographic detail
363 recorded/available. Jaboyedoff et al. (2004), using the same approach, developed a code designed to
364 integrate structural data into the digital surface model.

365 Limit equilibrium methods are routinely used to identify the slope hazard due to translational and
366 rotational movements occurring along a distinct failure surface(s). These analyses consider force and/or
367 moment equilibrium conditions and can be performed by stereonet, or preferably 2D/3D rock structure
368 models. They may also be used to provide a preliminary assessment of rock slope toppling failure.
369 Analyses are carried out to calculate either a Factor of Safety (FoS) or, through back analysis, a range of
370 shear strength parameters at failure. The results of this type of calculation are based on the geometry of
371 slope (or potential unstable block, depending on the scale of work), material properties, forces involved
372 (water pressure, seismic forces, external forces), and discontinuity mechanical properties. In this context
373 the use of remote sensing techniques play an important role in the definition of the discrete location of the
374 discontinuities that form the failure surface(s) and rear release (tension crack) of unstable blocks (a
375 necessary assumption in the limit equilibrium methods), the shape of the potentially unstable block and
376 thereby the true potential failure volume (Salvini et al. 2011; 2013). Figure 11 shows an example of this
377 method applied to a rock slope located in Northern Italy along the Domodossola-Iselle railway (after

378 Salvini et al., 2011). Using a photogrammetric survey carried out with a helicopter (Figure 11A), detailed
379 photographs of the rock slopes were acquired (Figure 11B) allowing definition of the geometry of blocks
380 and discontinuities (Figure 11C). This information was used to calculate the deterministic FoS using limit
381 equilibrium software (Figure 11D).

382 The volume of blocks, together with the location (in term of coordinates) of each potential unstable block
383 can also be used for rockfall simulation. Rockfall analysis is based on the study of the slope geometry and
384 the characteristics of potential falling blocks. It is possible to determine the kinetic energy, velocity,
385 "bounce height", end points and lateral dispersion of potential falling blocks for the entire slope. Having a
386 good representation of the slope morphology, potential unstable block geometry and land cover is crucial
387 for this type of simulation. Figure 12 shows an example of combined use of remote DP and rockfall run
388 out simulation in the Grotta delle Felci Cliff (Capri Island, Italy). The location (Figure 12A) and geometry
389 (Figure 12C) of rock blocks were determined from a helicopter based photogrammetric survey and the
390 data used for an improved understanding of the lateral dispersion of the potentially unstable blocks
391 (Figure 12B) in addition to their kinetic energy, velocity and "bounce height" (Figure 12D). This
392 approach can be very important in planning protection work (either active or passive), or proposing
393 monitoring systems (Salvini et al., 2011; 2013). Rockfall modelling represents a very powerful tool for
394 the study of risk mitigation, especially where rock slopes are located above infrastructure such as roads,
395 train tracks and working areas. Moreover, multi-temporal survey (e.g. with DP, LS, LiDAR and Radar
396 Interferometry) can be used for defining debris volume and for change detection (spatial and temporal)
397 analyses (Rosser et al., 2007; Blasone et al., 2014); thermal images and/or LS data can be used to locate
398 seepage that can be included in both conventional or more sophisticated analyses (Vivas et al., 2013;
399 Gigli et al., 2014).

400 **4.2 Remote sensing and more sophisticated numerical methods of slope analysis**

401 Although limit equilibrium methods are the simplest and most widely used slope analysis technique their
402 use should, in general, be limited to uncomplicated case studies. More sophisticated numerical methods
403 are better suited for the study of slopes of more complex slope geometry and structural geology.
404 Similarly, material anisotropy, non-linear behaviour, in situ stress, groundwater and brittle fracture can all
405 influence the slope stability and often can only be realistically considered using sophisticated numerical
406 simulations. These techniques of analysis, usually called numerical modelling analyses, can benefit
407 significantly from remote sensing data, especially where 3D variations in the slope geometry and
408 structure are important in the slope behaviour. Currently the most widely used 3D numerical codes for
409 slope stability analysis are Continuum (Finite Difference and Finite Element) and Discontinuum (Distinct
410 Element) codes. Havaej et al. (2015) describe the application of a recently introduced 3D lattice-spring
411 code that utilizes a lattice-based structure, consisting of point masses (nodes) connected by springs. The
412 lattice-spring model simulates rock fracture through the breakage of springs in shear and tension and once
413 the spring fails in either tension (normal spring) or shear (shear spring), the tensile strength and cohesion
414 reduce to zero (Havaej et al. 2015).

415 The advantages of the combined use of remote sensing and 3D Distinct Element Methods (DEM) in rock
416 slope investigations have been recently described by Francioni et al. (2014) and Spreafico et al. (2015).
417 Figure 13 shows an analysis undertaken using two models (with different spatial resolution) of the same

418 slope using a DEM. The principal objective of the study by Francioni et al. 2014 was to highlight the
419 advantages and limitations of using terrestrial remote sensing data in a 3D DEM. The first model was
420 obtained from a topographic map (Figure 13A, B and C) and the second model from terrestrial LS (Figure
421 13D, E and F). These simulations demonstrated that the values of Strength Reduction Factor (SRF)
422 obtained from the stability analysis can be significantly influenced by the measured geometry of the slope
423 (Francioni et al., 2014).

424 The use of remote sensing data and the 3D Finite Difference Method (FDM) was illustrated by Francioni
425 et al. (2015) in order to understand the stress-induced damage in surface mined areas. Simulations were
426 undertaken using the slope geometry derived from DP and LS. In this case, it was possible to increase the
427 understanding of stress-induced damage in the Lorano open pit (Carrara, Italy) due to the excavation
428 processes (Figure 14A-B). The detailed information on the structural geological setting of the entire slope
429 obtained from DP and LS was also used in DEM analysis. Measured data from a conventional
430 engineering geological survey (e.g. scan line or window) can often only be used in discontinuum
431 modelling of simple rock slopes assuming continuous or persistent joint sets. The data determined from
432 remote sensing techniques however can allow for more sophisticated deterministic (using only joints
433 visible on the DP/LS model) or stochastic Discrete Fracture Network, DFN, analyses. Figure 15 shows
434 the differences between the DEM models created using continuous joint sets (Figure 15 A-B) and a DFN
435 (Figure 15 C-D).

436 It must be emphasized, however, that the time needed for data processing are significantly longer when
437 dealing with accurate and detailed slope geometry and that such detailed data is useful in complex cases
438 but may be unnecessary in simple slopes where a large scale topographic map can still be suitable
439 (Francioni et al., 2014). Havaej et al. (2016) clearly showed the advantages of using terrestrial
440 photogrammetry and LIDAR in developing DFN for a slate quarry slope at Delabole, Cornwall, UK.
441 Detailed data were used to investigate the influence of different stochastic generated DFN's on simulated
442 slope failure mechanisms, the results agreeing with observed slope behaviour.

443 Havaej et al. (2015) showed the use of ground-based photogrammetric and airborne LiDAR data in the
444 analysis of the Vajont slide, Italy, using a lattice-spring approach. The landslide model was built using the
445 airborne LiDAR data while the sliding surface, discontinuity orientations and locations were derived from
446 combined field analysis and long-range terrestrial photogrammetry. The use of this 3D-brittle fracture
447 software, together with airborne and terrestrial remote sensing data, allowed the authors to improve the
448 understanding of the importance of kinematics, internal damage and groundwater levels on the failure of
449 the 1963 Vajont slide.

450 Wang et al. (2003) and Lorig et al. (2009) showed the use of particle flow codes for the analysis of rock
451 slopes. Although this method showed good results for 2D simulations, its use in 3D modelling remains
452 computationally expensive. Eberhardt et al. (2004) used hybrids methods, using a Finite Element mesh to
453 represent the intact joint bounded blocks and discrete elements to simulate joint behaviour to explain the
454 failure mechanism of the Randa rock slide (Switzerland) and Styles et al. (2011) applied it to the back
455 analysis of the Joss Bay Chalk cliff (UK). Vyazmensky et al. (2010) and Styles et al. (2011) incorporated
456 discrete fracture networks into hybrid numerical models to realistically simulate rock slope deformation
457 in the Palabora, South Africa and Bingham Canyon, US, open pits respectively.

458 As previously mentioned, apart from slope geometry information DP and LS can also be used for defining
459 discontinuity roughness angles and Joint Roughness Coefficient (Haneberg, 2007; Kim et al., 2015;
460 2016). Höfle et al. (2009), Kurz (2012) and Park et al. (2016) recently showed how it is possible use LS
461 intensity signal and hyperspectral imagery to locate seepage and rock weathering/alteration zones.
462 Moreover, rock mass heterogeneities can also be remotely detected to develop ubiquitous joint rock mass
463 models (Sainsbury et al. 2016).

464 **5 Final remarks and discussions**

465 In this paper, we show how remote sensing data can be successfully used to define the morphology and
466 structural setting of both natural and engineered slopes, the shape and volume of potential unstable blocks
467 and the geometry of the potential failure surfaces.

468 The selection of a specific survey technique for a given site remains a complex and challenging problem
469 which requires knowledge of the terrain, the objective of the project, the availability of funding and
470 technologies approved for use in the region (Lato et al., 2015). For this reason, it is important to recognize
471 that the methods described should wherever possible be considered as complementing each other rather
472 than being competitive.

473 In this context, Table 1 and 2 summarize respectively the DP and LS platforms currently available;
474 highlighting their advantages and limitations. Airplane and satellite generated data are not included in
475 these tables because as previously mentioned, due the nadir point of observation they are not optimal for
476 deterministic study of natural and engineered rock slopes. Figure 16 provides a comparison of the DP
477 remote sensing platforms discussed in this paper in relation to their cost, simplicity of use and ability to
478 avoid occlusions.

479 It has been shown how the information gained using these remote sensing techniques can be usefully
480 applied within different types of conventional and numerical analyses, and can play a key role in the final
481 results of the model simulations. Figure 17 presents additional information that can be retrieved with LS
482 and DP and the improvements in terms of input parameters that these techniques can offer conventional
483 and numerical analyses of slopes.

484 It should be noted that, wherever possible, integrated use of different remote sensing with conventional
485 mapping and monitoring investigation techniques is recommended as this allows for the validation of the
486 data and an understanding of the advantages and limitations of the proposed methodology.

487 The integration of slope monitoring systems with conventional and numerical analyses is a crucial aspect
488 in the study of landslides. This is highlighted by new research on slope monitoring using remote sensing
489 techniques that have been recently proposed by Sharma et al. (2016), Travelletti et al. (2016), Salvini et
490 al. (2015b) and Kromer et al. (2015a; b). The results obtained from this research will improve the
491 understanding of landslide behaviour.

492 **6 Conclusions**

493 This research presents international examples of the application of remote sensing techniques in the study
494 of rock slopes and landslides and highlights the importance of incorporating the data gained from these

495 techniques in subsequent stability analyses. We demonstrate the use of the different methods of remote
496 sensing surveys and illustrate how each data set can be important in improving the precision and
497 reliability of rock slope analyses.

498 With regard to DP, considerations of cost and flexibility often make the use of the hand-held camera or
499 tripod the most convenient and effective photogrammetric solution. UAV systems are however
500 increasingly seen as the preferred option as they are the least expensive aerial option and also provide the
501 maximum ability to avoid occlusions.

502 With regard to LS, their use is simple and the results are very precise and reliable (especially in the case
503 of full waveform LS). The cost of the equipment is the main limitation of these techniques especially
504 when compared with DP. Occlusions can still be a problem when dealing with very high slopes and
505 ground based platforms. UAV LS systems can overcome this problem but accuracy, precision and
506 resolution of data decrease considerably when compared with ground-based platforms.

507 All the described remote sensing survey techniques can provide data sets suitable for incorporation into
508 the varied methods of slope stability analysis. This data can overcome many limitations related to input
509 parameters and the difficulties in reducing model and parameter uncertainty. Multiple methods of
510 numerical analysis can be performed with remote sensing derived data and stochastic methods can be
511 used to perform multiple simulations in order to better calibrate model results.

512 In kinematic analysis, the use of remote sensing techniques can result in more representative structural
513 geological assessment of rock slopes; with continuing development in kinematic and block theory
514 approaches, remote sensing data will be more efficiently utilized in slope design and remediation.

515 In limit equilibrium analysis, the use of specific block and discontinuity geometry directly available from
516 DP and/or LS will lead to more reliable slope analyses as a result of decreased uncertainty related to the
517 block volume and discontinuity inclination. Moreover, the block volume, location and shape, together
518 with data concerning the slope geometry and land cover will also allow more detailed and realistic
519 rockfall runout simulations and the construction of more reliable hazard and risk maps.

520 Remote sensing data when incorporated into more sophisticated numerical models provides improved
521 slope geometry input and also the possibility to include deterministic and/or stochastic representation of
522 discontinuities (especially relevant to future improvements in the 3D analysis of complex slopes). This
523 allows improved analyses and increased scope for model calibration. However, the use of complex
524 geometry increases the simulation time significantly and it is important to understand when this approach
525 is necessary and when it can and should be avoided.

526 **Acknowledgements**

527 The authors wish to thank Ms. Megan Dewit and Ms. Allison Westin (Simon Fraser University, BC,
528 Canada) for their support during the remote sensing survey along the See to Sky Highway (BC, Canada).
529 We are extremely grateful to Dr. Silvia Riccucci for her assistance during the photogrammetric surveys in
530 the Carrara marble district and Northern Italy. Moreover, we would like to express our gratitude to the
531 reviewers who provided important and constructive suggestions for improving the quality of the paper.

References

- 533 – Afana, A., Williams, J.G., Hardy, R.J., Rosser, N.J., Hunter, G., Davis, J. 2013. Integrating full-
534 waveform terrestrial laser scanning into automated slope monitoring. Poster presented at XV
535 International ISM Congress 2013. 16-20 September, Aachen, Germany.
- 536 – Assali, P., Fivel, A., Pollet, N., Viguier, F. 2016. UAV systems for linear inspection. 3th
537 International Symposium Rock Slope stability, Lyon 2016. 119-120.
- 538 – Barbarella, M., Fiani, M., Lugli, A. 2015. Landslide monitoring using multitemporal terrestrial
539 laser scanning for ground displacement analysis. *Geomatics, Natural Hazards and Risk*, 6, 398-418.
- 540 – Beraldin, J. A., 2004. Integration of laser scanning and close-range photogrammetry— the last
541 decade and beyond. *Proceedings: XXth International Society for Photogrammetry and Remote*
542 *Sensing (ISPRS) Congress, Istanbul, Turkey*. 972-983.
- 543 – Besl, P., McKay. N., 1992. A Method for Registration of 3-D Shapes. *Institute of Electrical and*
544 *Electronic Engineers IEEE Transactions on Pattern Analysis and Machine Intel.* 14 (2), 239-256.
- 545 – Birch, J.S., 2006. Using 3DM Analyst mine mapping suite for rock face characterization. In: Tonon,
546 F. and Kottenstette, J. (Eds.), *Laser and Photogrammetric Methods for Rock Face Characterization*,
547 ARMA. 13-32.
- 548 – Blasone, G., Cavalli, M., Cazorzi, F., 2014. Debris-flow monitoring and geomorphic change
549 detection combining laser scanning and fast photogrammetric surveys in the Moscardo catchment
550 (Eastern Italian Alps). *Engineering Geology for Society and Territory*. 3, 51-54.
- 551 – Bonilla-Sierra, V., Scholtès, L., Donzé, F.V., Elmouttie, M. K. 2015. Rock slope stability analysis
552 using photogrammetric data and DFN–DEM modelling. *Acta Geotech.* 10, 497-511.
- 553 – Brideau, M., A., Stead, D., 2010. Controls on block toppling using a three-dimensional distinct
554 element approach. *Rock Mech Rock Eng.* 43, 241-260.
- 555 – Brideau M.A., Pedrazzini A., Stead D. Froese C., Jaboyedoff M., van Zeyl D., 2011. Three-
556 dimensional slope stability analysis of South Peak, Crowsnest Pass, Alberta, Canada. *Landslide*. 8,
557 139-158.
- 558 – Clayton, A., Stead, D., Kinakin, D., Wolter, A. 2017. Engineering geomorphological interpretation
559 of the Mitchell Creek Landslide, British Columbia, Canada. *Landslides*. In press.
- 560 – Clague J.J., Stead D., Francioni M., Westin A. 2015. *Geology of Mount Burnaby*. Unpublished
561 report for Kinder Morgan, Calgary, AB, 13pp.
- 562 – Colomina, I., Molina, P. 2014. Unmanned aerial systems for photogrammetry and remote sensing:
563 A review. 92, 79-97.
- 564 – Coggan, J.S., Wetherelt, A., Gwynn, X.P., Flynn, Z., 2007. Comparison of hand-mapping with
565 remote data capture systems for effective rock mass characterisation, 11th Congress of International
566 Society for Rock Mechanics, Lisbon 2007, 9th - 13th Jul 2007, *Proceedings of 11th Congress of*
567 *the International Society for Rock Mechanics - the second half century of rock mechanics*. 1, 201-
568 205.
- 569 – Copons, R., Vilaplana, J.M., 2008. Rock fall susceptibility zoning at a large scale: from
570 geomorphological inventory to preliminary land use planning. *Eng Geol.* 102 3-4, 142-151.
- 571 – Eberhardt, E., Stead, D., Coggan, J.S., 2004. Numerical analysis of initiation and progressive
572 failure in natural rock slopes—the 1991 Randa rockslide. *Int. J. Rock Mech. Min. Sci.* 41 (1), 69–
573 87.

- 574 – Donati, D., Stead, D., Ghirotti, M., Brideau, M-A. 2017. A model-oriented, remote sensing
575 approach for the derivation of numerical modelling input data: Insights from the Hope Slide,
576 Canada. Proc. ISRM International Symposium ‘Rock Mechanics for Africa’ AfriRock Conference
577 2017, Cape Town, S., SAIMM, 15pp.
- 578 – Elmo, D., 2006. Evaluation of a hybrid FEM/DEM approach for determination of rock mass
579 strength using a combination of discontinuity mapping and fracture mechanics modelling, with
580 particular emphasis on modelling of jointed pillars. Ph.D. thesis. Camborne School of Mines,
581 University of Exeter, UK.
- 582 – Eyre, M., Wetherelt, A., Coggan, J. 2016. Evaluation of automated underground mapping solutions
583 for mining and civil engineering applications. *J. Appl. Remote Sens.* 10(4), 046011 (Nov 16, 2016).
584 doi:10.1117/1.JRS.10.046011.
- 585 – Firpo, G., Salvini, R., Francioni, M., Ranjith, P.G., 2011. Use of digital terrestrial photogrammetry
586 in rocky slope stability analysis by distinct element numerical methods. *Int. J. Rock Mech. Min.*
587 *Sci.* 48 (7), 1045-1054.
- 588 – Francioni, M., Girgenti, C., Vanneschi, C. 2013 Underground quarrying industry and terrestrial
589 laser scanning. *Rendiconti Online Societa Geologica Italiana.* 24, pp. 140-142.
- 590 – Francioni, M., Salvini, R., Stead, D., Litrico, S. 2014. A case study integrating remote sensing and
591 distinct element analysis to quarry slope stability assessment in the Monte Altissimo area, Italy.
592 *Eng Geo.* 183, 290-302
- 593 – Francioni, M., Salvini, R., Stead, D., Giovannini, R., Riccucci, S., Vanneschi, C., Gullì, D. 2015.
594 An integrated remote sensing-GIS approach for the analysis of an open pit in the Carrara marble
595 district, Italy: Slope stability assessment through kinematic and numerical methods. *Computers and*
596 *Geotechnics* 67, 46-63.
- 597 – Fröhlich, C., Mettenleiter, M., 2004. Terrestrial laser scanning — new perspectives in 3D
598 surveying. In: Thies, M., Koch, B., Spiecker, H., Weinacker, H. (Eds.), *Laser-scanners for Forest*
599 *and Landscape Assessment.* International Archives of Photogrammetry, Remote Sensing and
600 Spatial Information Sciences. XXXVI-8/W2, 7-13.
- 601 – Ghirotti, M., Genevois, R., 2007. A complex rock slope failure investigated by means of numerical
602 modelling based on laser scanner technique. In *Proceedings: 1st Canada-US Rock Mechanics*
603 *Symposium.* May 27-31, Vancouver, 917-924.
- 604 – Gauthier, D., Hutchinson, J., Lato, M., Edwards, T., Bunce, C., Wood, D. 2015. On the precision,
605 accuracy, and utility of oblique aerial photogrammetry (OAP) for rock slope monitoring and
606 assessment. 68th Canadian Geotechnical Conference. GeoQuebec, September 20-23, 2015.
- 607 – GigaPan 2016. GigaPan Systems: <http://www.gigapan.com/>.
- 608 – Gigli, G., Frodella, W., Garfagnoli, F., Morelli, S., Mugnai, F., Menna, F., Casagli, N. 2014. 3-D
609 geomechanical rock mass characterization for the evaluation of rockslide susceptibility scenarios.
610 *Landslides.* 11, 131-140.
- 611 – Haarbrink, R.B., Eisenbeiss, H., 2008. Accurate DSM production from unmanned helicopter
612 systems. International Archives of Photogrammetry, Remote Sensing and Spatial Information
613 Sciences. XXXVII/B1. PRC, Beijing, 159-164.
- 614 – Haneberg W.C., Norrish, N.I., Findley, D.P., 2006. Digital outcrop characterization for 3-D
615 structural mapping and rock slope design along Interstate 90 near Snoqualmie Pass, Washington.

- 616 Proceedings 57th Annual Highway Geology Symposium, Breckenridge, Colorado, September 27-
617 29, 2006. pp. 1-14.
- 618 – Haneberg, W.C., 2007. Directional roughness profiles from three-dimensional photogrammetric or
619 laser scanner point clouds. In: Eberhardt, E., Stead, D., Morrison, T. (Eds.), Proceedings 1st
620 Canada-US Rock Mechanics Symposium. Vancouver, May 27-31, 2007, 101-106.
- 621 – Hamdi, P., Stead, D. and Elmo, D. 2015. Characterizing the influence of stress-induced microcracks
622 on the laboratory strength and fracture development in brittle rocks using a finite/discrete element
623 method-micro discrete fracture network FDEM- μ DFN approach, *Journal of Rock Mechanics and*
624 *Geotechnical Engineering*. 7, 509-625.
- 625 – Havaej, M., Wolter, A., Stead, D. 2015. The possible role of brittle rock fracture in the 1963 Vajont
626 Slide, Italy. *Int. J. Rock Mech. Min.* 78, 319-330.
- 627 – Havaej, M., Coggan, J., Stead, D., Elmo, D. 2016. A combined remote sensing–numerical
628 modelling approach to the stability analysis of Delabole Slate Quarry, Cornwall, UK. *Rock Mech*
629 *Rock Eng.* 49 (4), 1227-1245.
- 630 – Höfle, B., Vetter, M., Pfeifer, N., Mandlbürger, G., Stötter, J. (2009) Water surface mapping from
631 airborne laser scanning using signal intensity and elevation data. *Earth Surf Proc Land*. 34(12),
632 1635-1649.
- 633 – Oppikofer, T. 2009. Detection, analysis and monitoring of slope movements by high-resolution
634 digital elevation models. PhD thesis, Institute of Geomatics and Analysis of Risk, University of
635 Lausanne, Lausanne, Switzerland, 377 p.
- 636 – Jaboyedoff, M., Oppikofer, T., Abellan, A., Derron, M. E., Loye, A., Metzger, R., Pedrazzini, A.
637 2012. Use of LIDAR in landslide investigations: A review. *Natural Hazards* 61, 5-28.
- 638 – Jaboyedoff M, Baillifard F, Couture R, Locat J, Locat P. 2004. Toward preliminary hazard
639 assessment using DEM topographic analysis and simple mechanic modeling. In: Lacerda WA,
640 Ehrlich M, Fontoura AB, Sayo A (eds) Proceedings of the 9th International symposium on
641 landslides. Balkema, Rotterdam, pp 191-197
- 642 – Kim, D.H., Gratchev, I., Hein, M., Balasubramaniam, A. 2016. The application of normal stress
643 reduction function in tilt tests for different block shapes. *Rock Mech Rock Eng.* 49 (8), 3041-3054.
- 644 – Kim, D.H., Poropat, G.V., Gratchev, I., Balasubramaniam, A. 2015. Improvement of
645 photogrammetric JRC data distributions based on parabolic error models. *Int. J. Rock Mech. Min.*
646 *Sci.* 80,19-30.
- 647 – Kromer, R.A.; Abellán, A.; Hutchinson, D.J.; Lato, M.; Edwards, T.; Jaboyedoff, M. 2015a. A 4D
648 Filtering and Calibration Technique for Small-Scale Point Cloud Change Detection with a
649 Terrestrial Laser Scanner. *Remote Sens.* 7, 13029-13052.
- 650 – Kromer, R.A., Hutchinson, D.J., Lato, M.J. Gauthier, D., Edwards, T. 2015b. Identifying rock slope
651 failure precursors using LiDAR for transportation corridor hazard management. *Eng Geo.* 195, 93-
652 103.
- 653 – Kurz T.H., Buckley, S. J., Howell, J.A. 2012. Close range hyperspectral imaging integrated with
654 terrestrial LiDAR scanning applied to rock characterisation at centimetre scale. *International*
655 *Archives of the Photogrammetry, Remote Sensing and Spatial Information Sciences*, Volume
656 XXXIX-B5, 2012, XXII ISPRS Congress, 25 August – 01 September 2012, Melbourne, Australia.

- 657 – Lato, M., Diederichs, M.S., Hutchinson, D.J., Harrap, R., 2009. Optimization of LiDAR scanning
658 and processing for automated structural evaluation of discontinuities in rock masses. *Int. J. Rock*
659 *Mech. Min. Sci.* 46, 194-199.
- 660 – Lato, M.J., Gauthier, D., Hutchinson, D.J. 2015. Rock slopes asset management: Selecting the
661 optimal three-dimensional remote sensing technology. *Transportation Research Record.* 2510, 7-
662 14.
- 663 – Lato, M., Porter, M., Hensold, G., McDougall, S., Kromer, R., Gaib S. 2016. Understanding
664 landslide movement and kinematics with airborne Lidar, *Proc. Canadian, Geotechnical Conference,*
665 *GeoVancouver 2016,* 7pp.
- 666 – Lorig, L., Stacey, P., Read, J., 2009. Slope design methods. In: Read, J., Stacey, P. (Eds.),
667 *Guidelines for Open Pit Slope Design.* CSIRO Publishing, Collingwood, 237-264.
- 668 – Lucieer, A., Jong, S.M., Turner, D. 2014. Mapping landslide displacements using Structure from
669 Motion (SfM) and image correlation of multi-temporal UAV photography. *Progress in Physical*
670 *Geography.* 38 (1), 97-116.
- 671 – Mantovani, M., Devoto, S., Piacentini, D., Prampolini, M., Soldati, M., Pasuto, A. 2016. Advanced
672 SAR interferometric analysis to support geomorphological interpretation of slow-moving coastal
673 landslides (Malta, Mediterranean Sea). *Remote Sensing.* 8(6), 443.
- 674 – Michoud, C., Carrea, D., Costa, S., Derron, M.H., Jaboyedoff, M., Delacourt, C., Maquaire, O.,
675 Letortu, P., Davidson, R. 2015. Landslide detection and monitoring capability of boat-based mobile
676 laser scanning along Dieppe coastal cliffs, Normandy. 12 (2) 403-418.
- 677 – Niethammer, U., Rothmund S., James M. R., Travelletti J., Joswig M., 2010. UAV-based remote
678 sensing of landslides. *International Archives of Photogrammetry, Remote Sensing and Spatial*
679 *Information Sciences,* Vol. XXXVIII, 5.
- 680 – Piacentini, D., Devoto, S., Mantovani, M., Pasuto A., Prampolini, M., Soldati, M. 2015. Landslide
681 susceptibility modeling assisted by Persistent Scatterers Interferometry (PSI): an example from the
682 northwestern coast of Malta. *Nat Hazards* 78, 681-697.
- 683 – Park, J., Bates, M., Jeong, Y. S., Kim, K. M. Kemeny, J., 2016. Creating a digital outcrop model
684 by using hyper-spectrometry and terrestrial LiDAR. 50th U.S. Rock Mechanics/Geomechanics
685 Symposium. 26-29 June, Houston, Texas. ARMA-2016-507.
- 686 – Riegl, 2014. <http://www.riegl.com/>,
- 687 – Rosser, N., Lim, M., Petley, D., Dunning, S., Allison, R. 2007. Patterns of precursory rockfall prior
688 to slope failure. *Journal of Geophysical Research: Earth Surface.* 112 (4), F04014.
- 689 – Sainsbury, D. P., Sainsbury B. L., Sweeney, E. 2016. Three-dimensional analysis of complex
690 anisotropic slope instability at MMG’s Century Mine. *Mining Technology,* 125:4, 212-225.
- 691 – Salvini, R., Francioni, M., Fantozzi, P.L., Riccucci, S., Bonciani, F., Mancini, S., 2011. Stability
692 analysis of “Grotta delle Felci” Cliff (Capri Island, Italy): structural, engineering–geological,
693 photogrammetric surveys and laser scanning. *B Eng Geol Environ.* 70, 549-557.
- 694 – Salvini, R., Francioni, M. 2013. Geomatics for slope stability and rock fall runout analysis: a case
695 study along the Alta Tambura road in the Apuan Alps (Tuscany, Italy). *Italian Journal of*
696 *Engineering Geology.* 5, 481-492.
- 697 – Salvini, R., Francioni, M., Riccucci, S., Bonciani, F., Callegari, I., 2013. Photogrammetry and laser
698 scanning for analyzing slope stability and rock fall runout along the Domodossola–Iselle railway,
699 the Italian Alps. *Geomorphology.* 185, 110-122.

- 700 – Salvini R., Riccucci S., Gulli D., Giovannini R., Vanneschi C. and Francioni M. 2015a.
701 Geological application of UAV photogrammetry and terrestrial laser scanning in marble
702 quarrying (Apuan Alps, Italy). *Engineering Geology for Society and Territory - Volume 5*: 979 -
703 983.
- 704 – Salvini R., Vanneschi C., Riccucci S., Francioni, M., Gulli D., 2015b. Application of an integrated
705 geotechnical and topographic monitoring system in the Lorano marble quarry (Apuan Alps, Italy).
706 *Geomorphology*. 241, 209-223.
- 707 – Sharma, J., Francioni M., Busler J., Stead D., Donati D., Onsel E., Clague J., Brideau M-A. 2016.
708 Monitoring landslides in pipeline corridors using a combined satellite-based InSAR and
709 geomechanical modelling approach. *GeoVancouver 2016*. The 69th Canadian Geotechnical
710 Conference, 11 pp.
- 711 – Spreafico, M.C., Francioni, M., Cervi, F., Stead, D., Bitelli, G., Ghirelli, M., Girelli, V.A., Lucente,
712 C.C., Tini, M.A., Borgatti, L., 2016. Back analysis of the 2014 San Leo landslide using combined
713 terrestrial laser scanning and 3D distinct element modelling. *Rock Mechanics and Rock*
714 *Engineering*. 49, 2235-2251.
- 715 – Spreafico, M.C., Cervi, F., Francioni, M., Stead, Borgatti, L., 2017. An investigation into the
716 development of toppling at the edge of fractured rock plateaux using a numerical modelling
717 approach. *Geomorphology*. 288, 83-98.
- 718 – Stead, D., Eberhardt, E., Coggan, J.S., 2006. Developments in the characterization of complex rock
719 slope deformation and failure using numerical modelling techniques. *Eng Geo*. 83, 217-235.
- 720 – Stead, D., Coggan, J. 2012. Numerical modelling of rock slope stability. Book Chapter, In
721 "Landslide: Types, mechanisms and modelling", Eds Clague, J. and Stead D.; Cambridge
722 University Press., Chapter 13, 144-158.
- 723 – Stead, D., Wolter, A. 2015. A critical review of rock slope failure mechanisms: The importance of
724 structural geology. *Journal of Structural Geology*. 74, 1-23.
- 725 – Sturzenegger, M., Stead, D., 2009(a). Close-range terrestrial digital photogrammetry and terrestrial
726 laser scanning for discontinuity characterization on rock cuts. *Engineering Geology* 106, 163-182.
- 727 – Sturzenegger, M., Stead, D., 2009(b). Quantifying discontinuity orientation and persistence on high
728 mountain rock slopes and large landslides using terrestrial remote sensing techniques. *Natural*
729 *Hazards and Earth System Sciences*. 9 (2), 267-287.
- 730 – Sumnall, M.J., Hill, R.A., Hinsley, S.A. 2016. Comparison of small-footprint discrete return and
731 full waveform airborne lidar data for estimating multiple forest variables. *Remote Sensing of*
732 *Environment*. 173, 214-223.
- 733 – Styles, T., Coggan, J.S., Pine, R.J. 2011. Back analysis of the Joss Bay Chalk Cliff Failure using
734 numerical modelling. *Engineering Geology*, 120(1): 81-90.
- 735 – Styles, T., Rabus, B., Bloom, J. 2011. Integrated numerical modelling and InSAR monitoring of a
736 slow moving slope instability at Bingham Canyon Mine. *Slope Stability 2011, International*
737 *Symposium on Rock Slope Stability in Open Pit Mining and Civil Engineering, Vancouver,*
738 *Canada*, 10 pp.
- 739 – Take, W. A., Chappel, M. J., Brachman, R. W. I., Rowe, R. K. 2007. Quantifying geomembrane
740 wrinkles using aerial photography and digital image processing. *Geosynthetics International*. 14,
741 14(4), 219-227

- 742 – Travelletti, J., Philippoussian, F., Mayoraz, R., 2016. A cost-efficient approach to monitor rockfall
743 activity over large areas using non-permanent single-camera system (mono-photogrammetry). 3th
744 International Symposium Rock Slope stability, Lyon 2016. 135-136.
- 745 – Tuckey, Z., Stead, D. and Eberhardt, E. 2013. An Integrated Approach for Understanding
746 Uncertainty of Discontinuity Persistence and Intact Rock Bridges in Large Open Pit Slopes, Proc.
747 Slope Stability 2013. Brisbane, Sept 2013, 189-204.
- 748 – Vallet, J., Skaloud, J., Kölbl, O., Merminod, B. 2000. Development of a helicopter based integrated
749 system for avalanche and hazard management. International Archives of Photogrammetry and
750 Remote Sensing. 33 B2, 565-572.
- 751 – Vivas, J., Tuckey, Z., Stead, D., Wolter, A., Elmo, D. and D'Ambra, S. 2013. Seepage
752 characterization in high rock slopes using remote sensing, Proc. ARMA, San Francisco ARMA
753 Paper No. 13-462, 19pp.
- 754 – Vyazmensky, A., Stead, D., Elmo, D., Moss, A. 2010. Numerical analysis of block caving-induced
755 instability in large open pit slopes: A finite element/discrete element approach. Rock Mechanics
756 and Rock Engineering, 43 (1), 21-39.
- 757 – Westin, A.M. 2017. Downie Slide: An integrated remote sensing approach to characterization of a
758 very slow moving landslide; MSc. Thesis, Simon Fraser University
- 759 – Westoby, M.J., Brasington J., Glasser, N.F., Hambrey, M.J., Reynolds J.M. 2012. 'Structure-from-
760 Motion' photogrammetry: A low-cost, effective tool for geoscience applications. Geomorphology.
761 179, 300-314
- 762 – Wolter, A., Stead, D., Ward, B.C., Clague, J.J., Ghirotti, M. 2016. Engineering geomorphological
763 characterisation of the Vajont Slide, Italy, and a new interpretation of the chronology and evolution
764 of the landslide. Landslides. 5, 1067-1081.

765

766 **Figure Captions:**

767 Figure 1. Photogrammetric acquisition methods (Birch, 2006) and Structure from Motion. A) Independent
768 convergent model. B) Image fan method. C) Image strip method. D) Structure from Motion.

769 Figure 2. Photogrammetric image acquisition using A) a tripod and B) a tripod with a reamed bar.

770 Fig 3. Full Waveform LS survey of a road cut along the Sea to Sky Highway, BC, Canada. A) RGB
771 colored slope model. B) Wave amplitude colored slope model.

772 Figure 4. LS survey. A) RGB photograph. B) RGB point cloud. C) Different registered echoes from
773 natural targets.

774 Figure 5. Equipment used for Digital Terrestrial Photogrammetry with an aerostatic balloon. A)
775 Aerostatic balloon. B) Two metre long photogrammetric frame (Francioni et al., 2014). C) Five metre
776 long photogrammetric frame (Firpo et al., 2011). D) Electrical winches for driving the system.

777 Figure 6. Equipment used for Digital Terrestrial Photogrammetry with a helicopter. A) Steel frame
778 adapted to fit a helicopter landing skid. B) Digital camera and GPS antennas. C) GPS data receivers and
779 laptop for real time photos visualization.

780 Figure 7. UAV survey (after Francioni et al., 2015). A) Falcon 8 UAV with gyro-stabilized digital camera
781 Sony NEX-5N. B) Drone during the flight.

782 Figure 8. A) 3D view of Mount Burnaby and Simon Fraser University, situated at the top of the mountain.
783 View to the southeast. B) 3D representations of LiDAR aspect maps with highlighted slump blocks on the
784 north face of Mount Burnaby. View to the southeast.

785 Figure 9. Kinematic slope stability analysis performed using A) Engineering geological data (93
786 measurements) and B) Remote sensing data (537 measurements) in the Lorano open pit (Carrara, Italy).

787 Figure 10. Lorano open pit. A) Photograph of the open pit buttress and B) SfM 3D model.

788 Figure 11. DP used for limit equilibrium analysis. A) Photogrammetric survey with a helicopter. B)
789 Example of detailed photographs acquired during the survey. C) Geometry of block and joints gained
790 from DP. D) Calculation of block FoS using DP data.

791 Figure 12. Use of DP data for defining the rockfall run out simulations. A) Location of potential unstable
792 blocks. B) Lateral dispersion of blocks in case of failure. C) Example of block geometry reconstruction
793 using the stereoscopy and the 3D modelling. D) 2D Simulation of block fall with possible calculation of
794 kinetic energy, velocity and "bounce height".

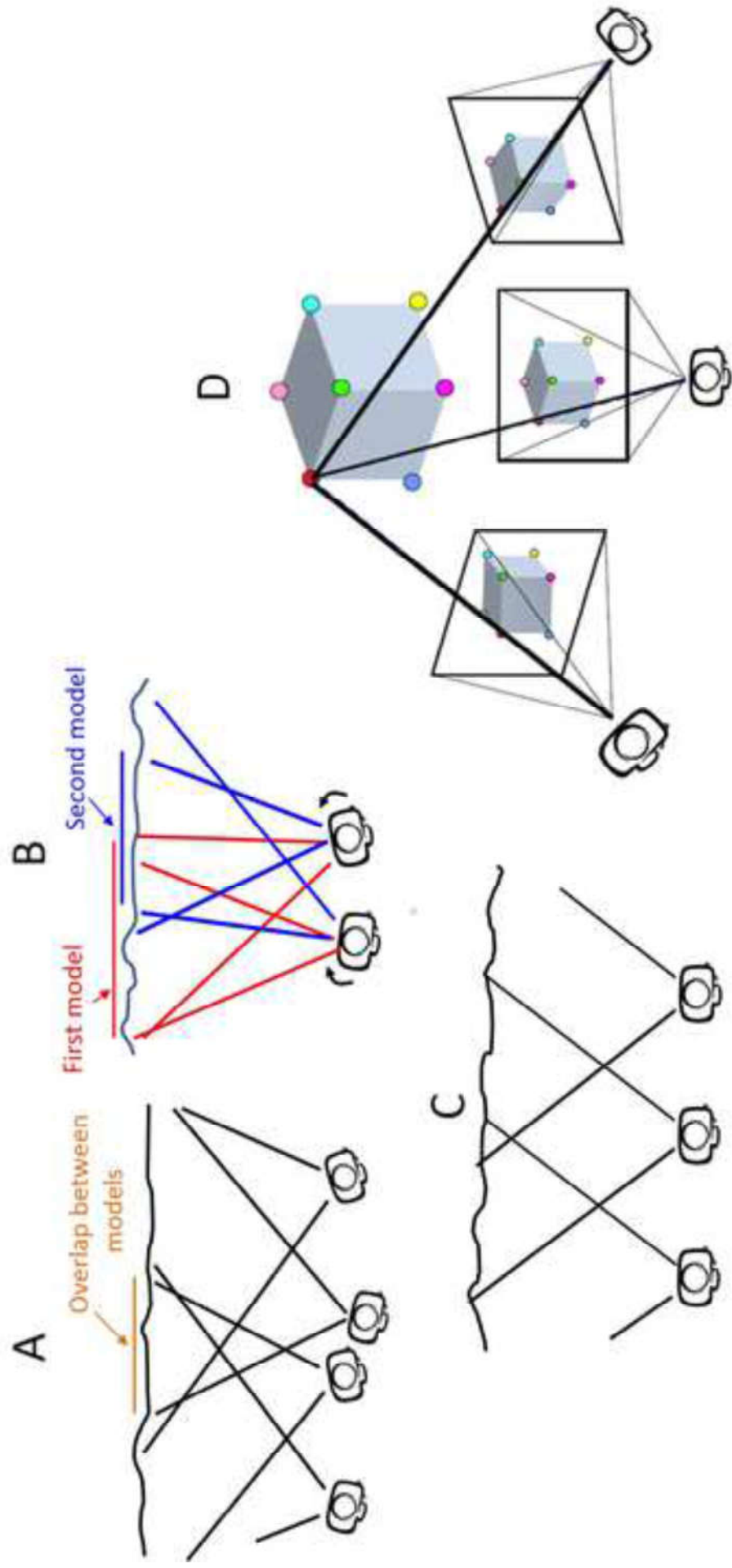
795 Figure 13. 3D rock slope models obtained from DP (after Francioni et al., 2014). A) Initial model from
796 topographic map B) 3D Distinct Element Model based on topographic map and C) 2D section, D) Initial
797 model from terrestrial laser scanning, E) 3D Distinct Element Model based on terrestrial laser scanning
798 and F) 2D section. Colours represent the distinct elements (blocks) generated by interaction between
799 different joint sets and the topography.

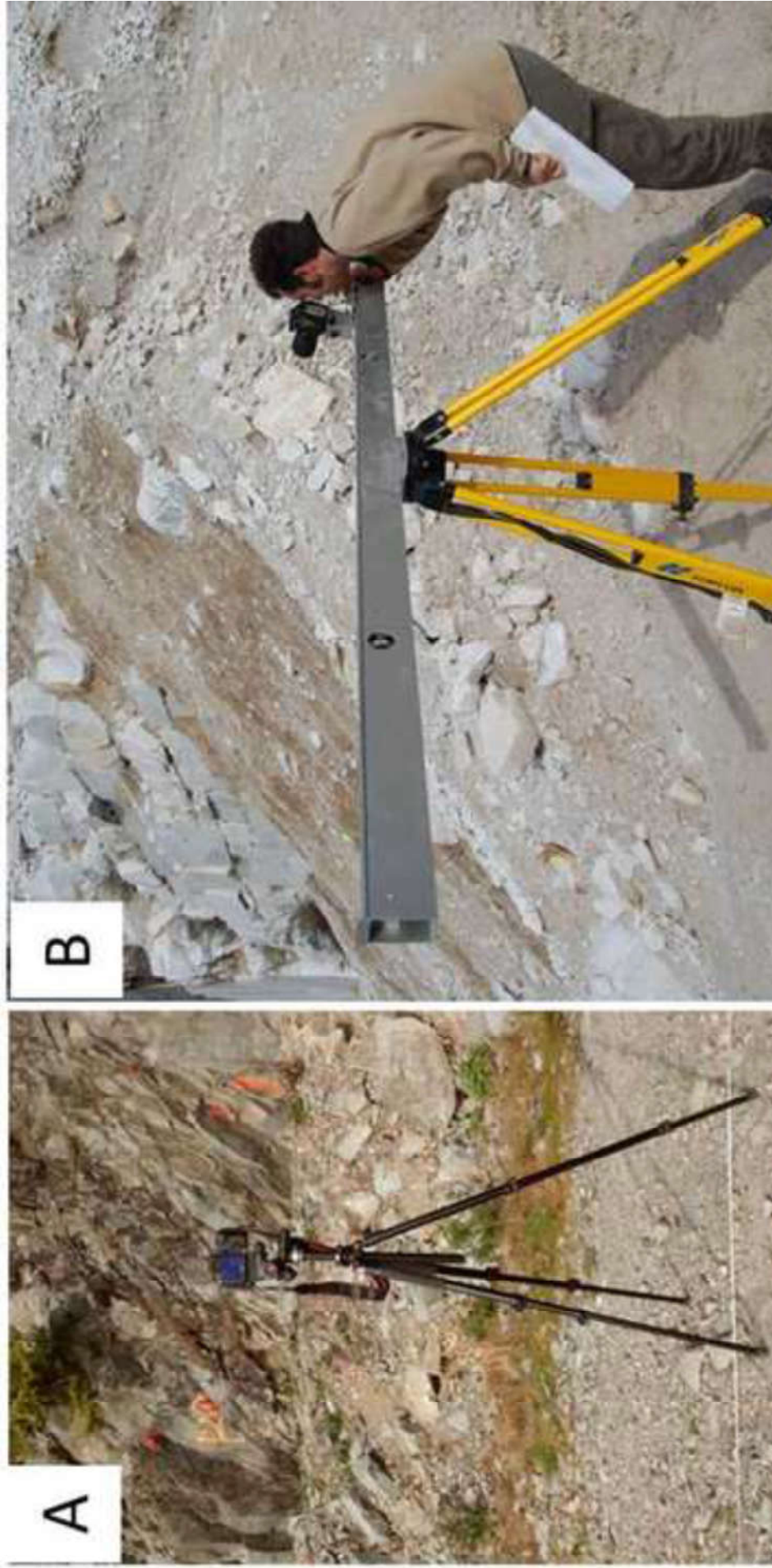
800 Figure 14. 3D rock slope models obtained from DP and LS (after Francioni et al. 2015). A) Initial model
801 and topography pre and post excavation. B) Stress analysis.

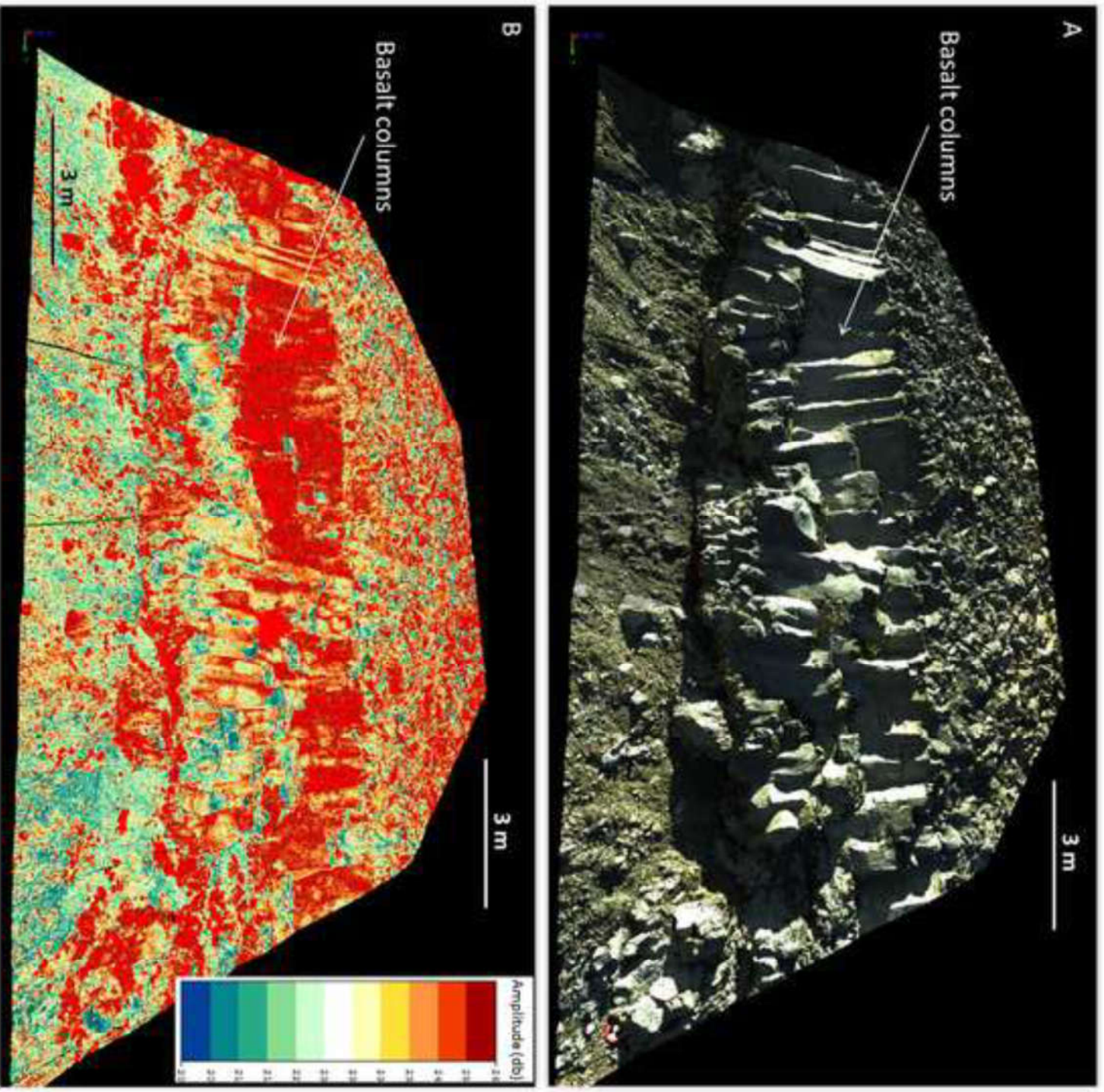
802 Figure 15. 3D rock slope models obtained from DP and LS. A) Initial 3DEC model. B) 3DEC model
803 using continuous persistent joint sets. C) 3DEC model using a deterministic approach. D) 3DEC model
804 using a stochastic DFN approach.

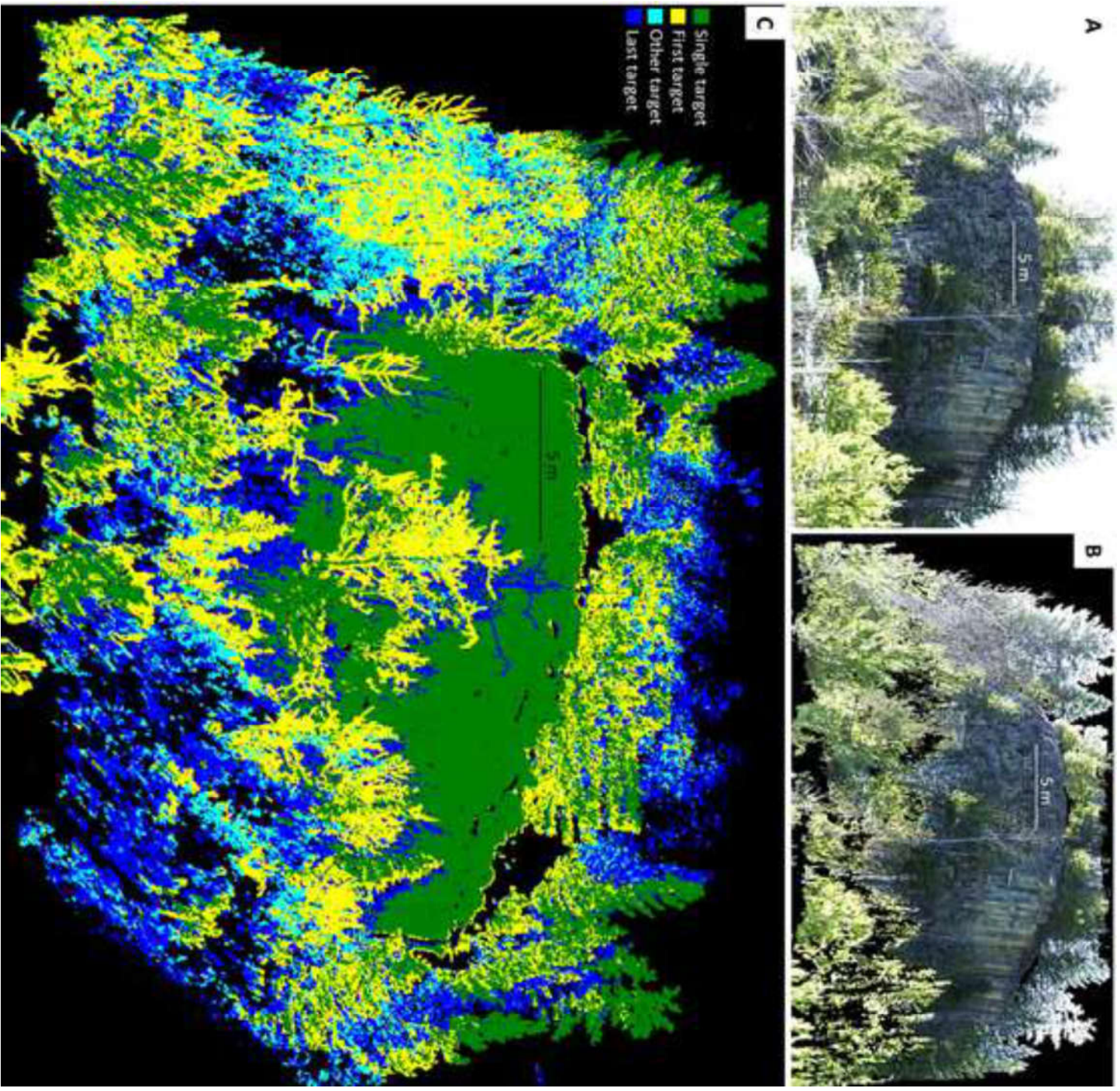
805 Figure 16. Comparison between DP platforms.

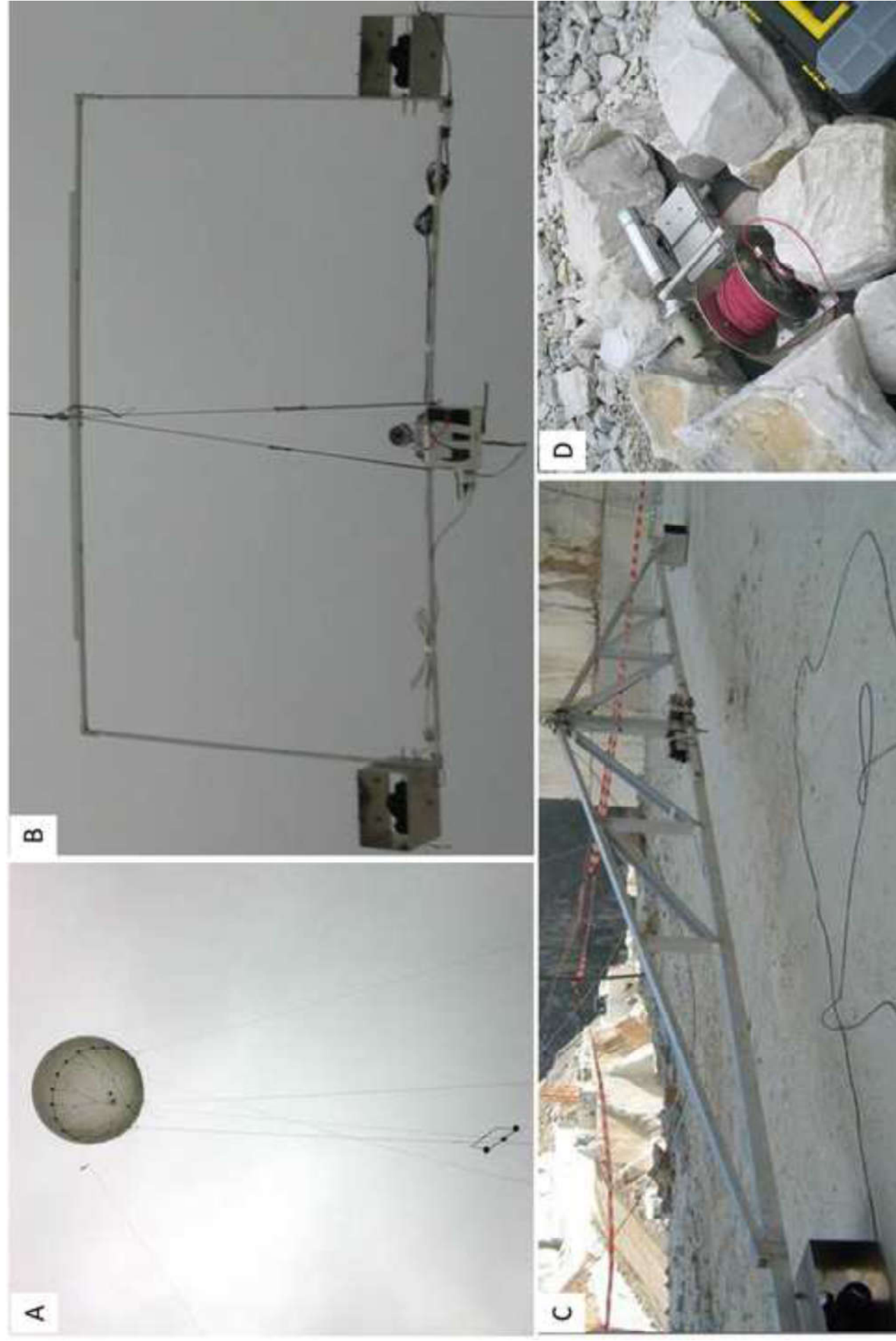
806 Figure 17. Improvement that geomatic techniques can offer in conventional and numerical slope analyses.





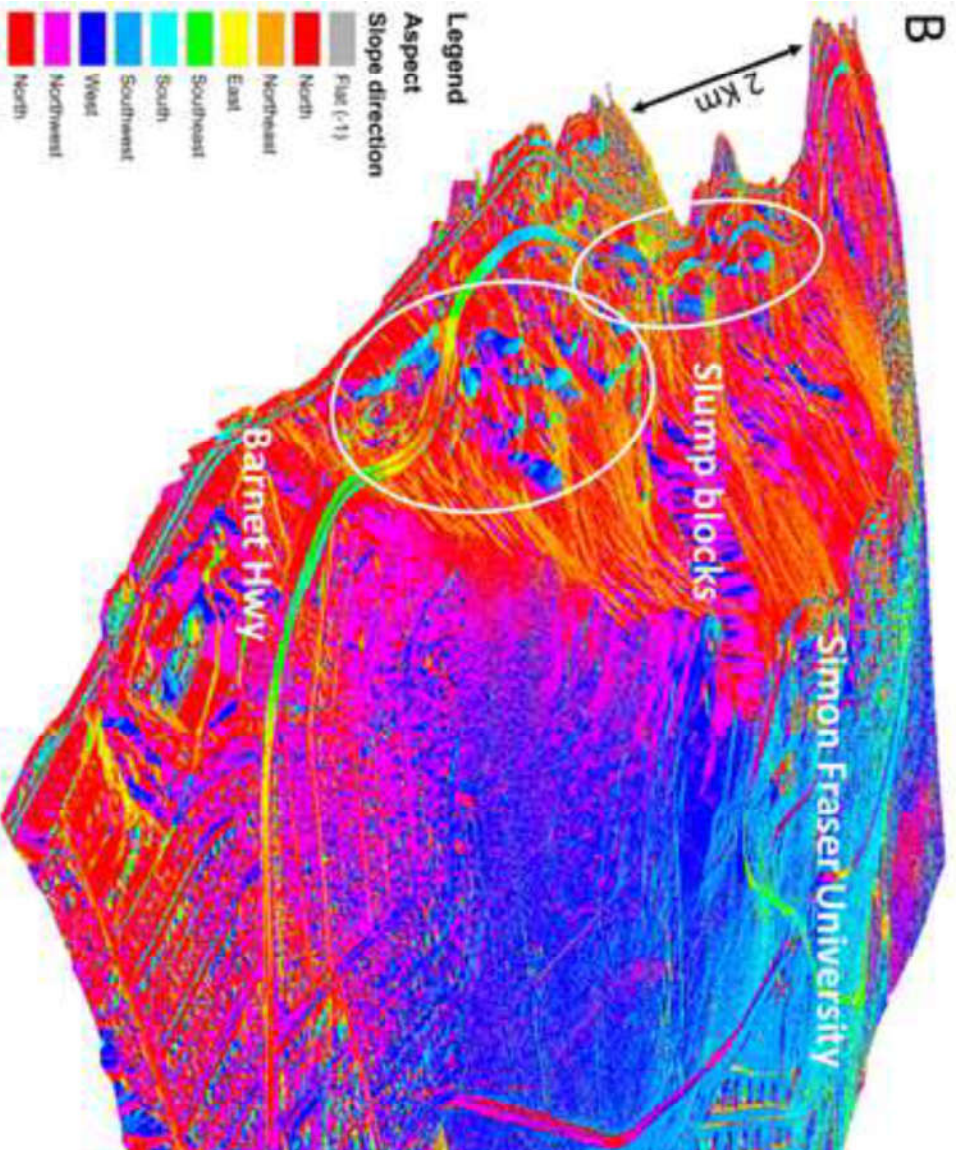


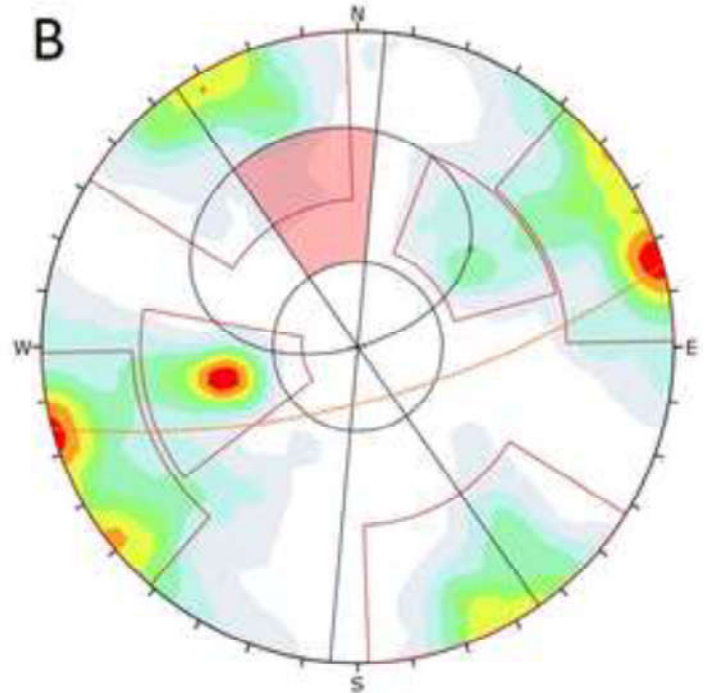
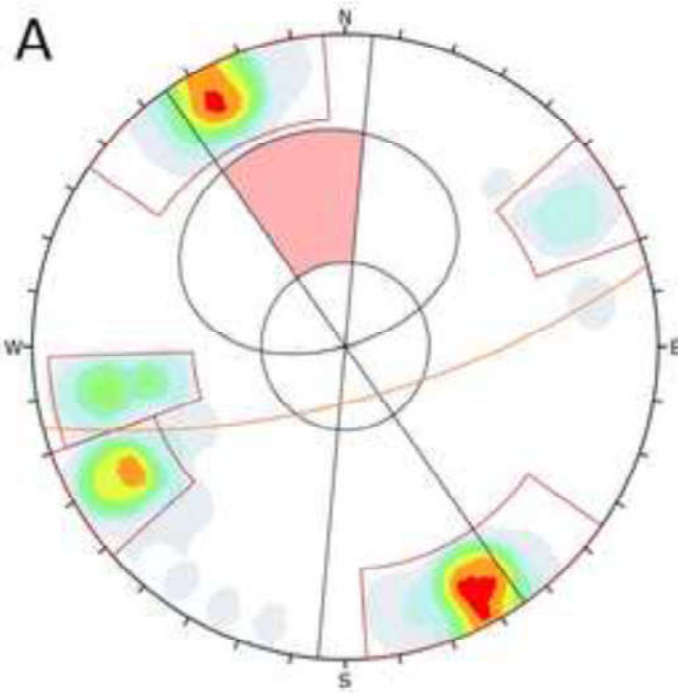












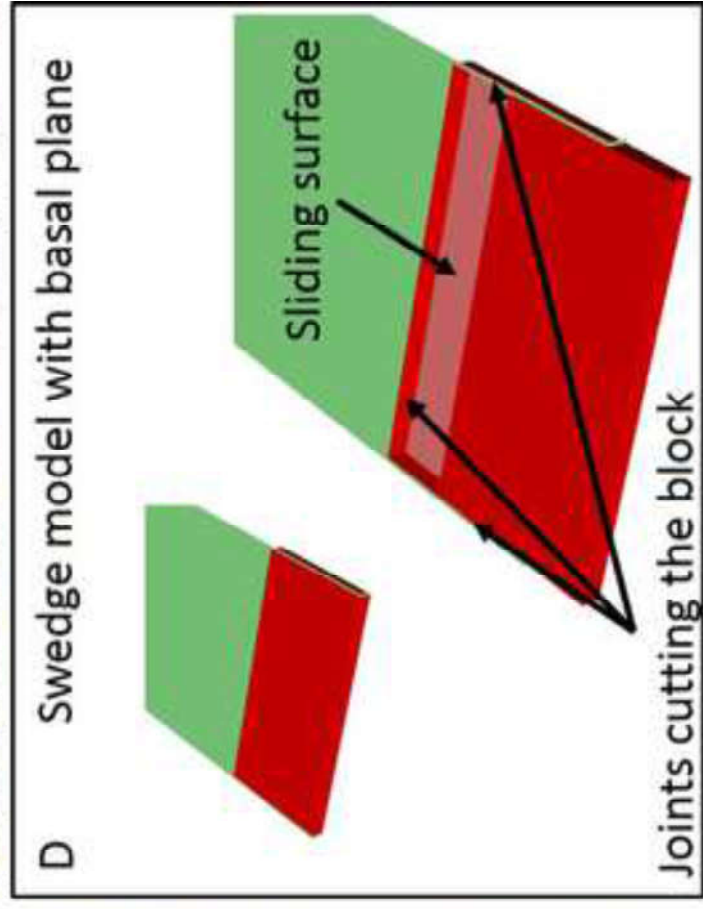
| Color | Density Concentrations |
|----------------------|------------------------|
| | 0.00 - 1.90 |
| | 1.90 - 3.80 |
| | 3.80 - 5.70 |
| | 5.70 - 7.60 |
| | 7.60 - 9.50 |
| | 9.50 - 11.40 |
| | 11.40 - 13.30 |
| | 13.30 - 15.20 |
| Contour Data | |
| Maximum Density | 14.20% |
| Contour Distribution | Fisher |
| Counting Circle Size | 1.0% |

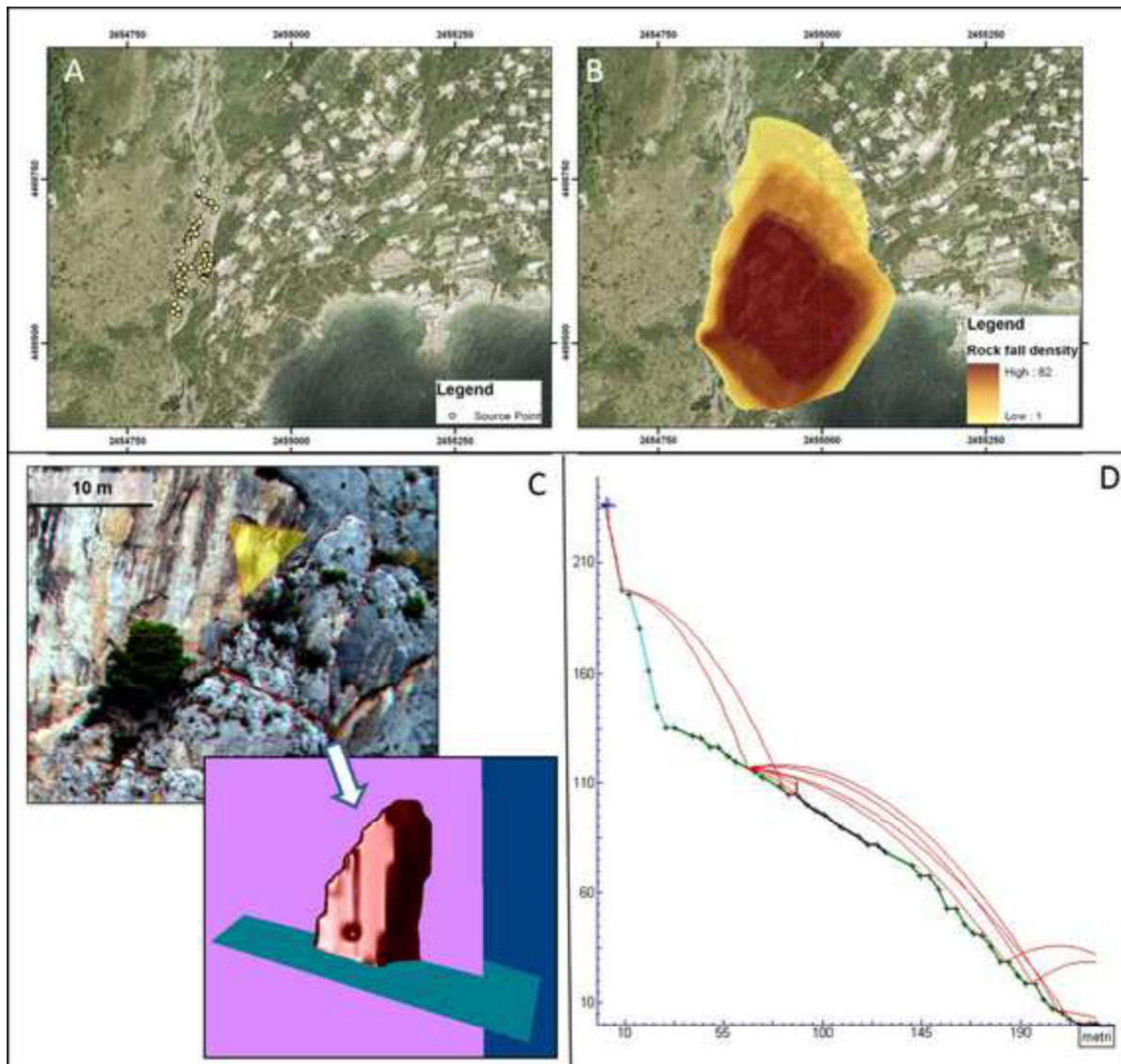
| Color | Density Concentrations |
|----------------------|------------------------|
| | 0.00 - 0.70 |
| | 0.70 - 1.40 |
| | 1.40 - 2.10 |
| | 2.10 - 2.80 |
| | 2.80 - 3.50 |
| | 3.50 - 4.20 |
| | 4.20 - 4.90 |
| | 4.90 - 5.60 |
| Contour Data | |
| Maximum Density | 5.49% |
| Contour Distribution | Fisher |
| Counting Circle Size | 1.0% |

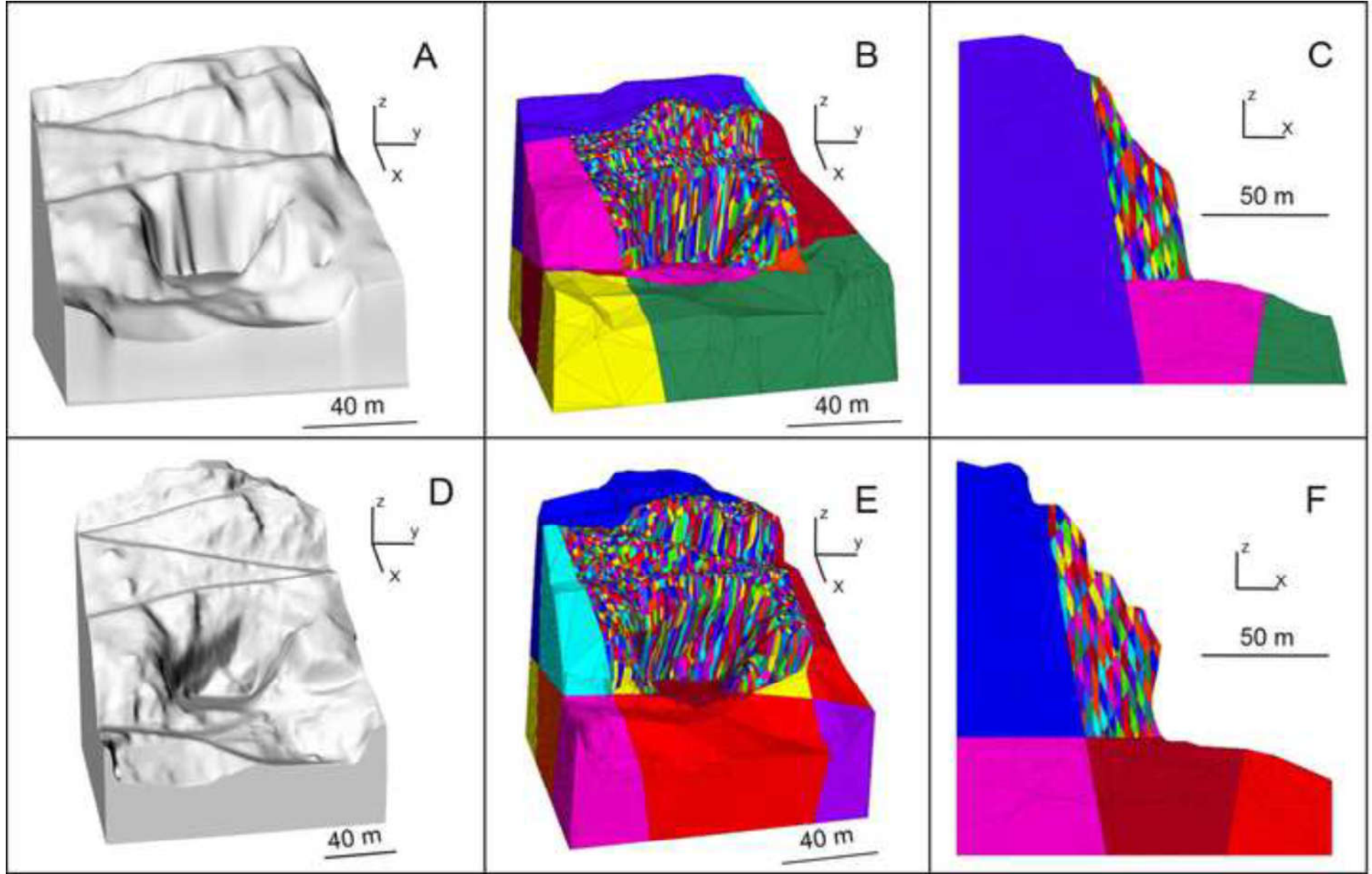
| Kinematic Analysis | Planar Sliding | | |
|----------------------|-----------------|--------------|----------|
| Slope Dip | 70 | | |
| Slope Dip Direction | 165 | | |
| Friction Angle | 30° | | |
| Lateral Limits | 20° | | |
| | Critical | Total | % |
| Planar Sliding (All) | 0 | 77 | 0.00% |

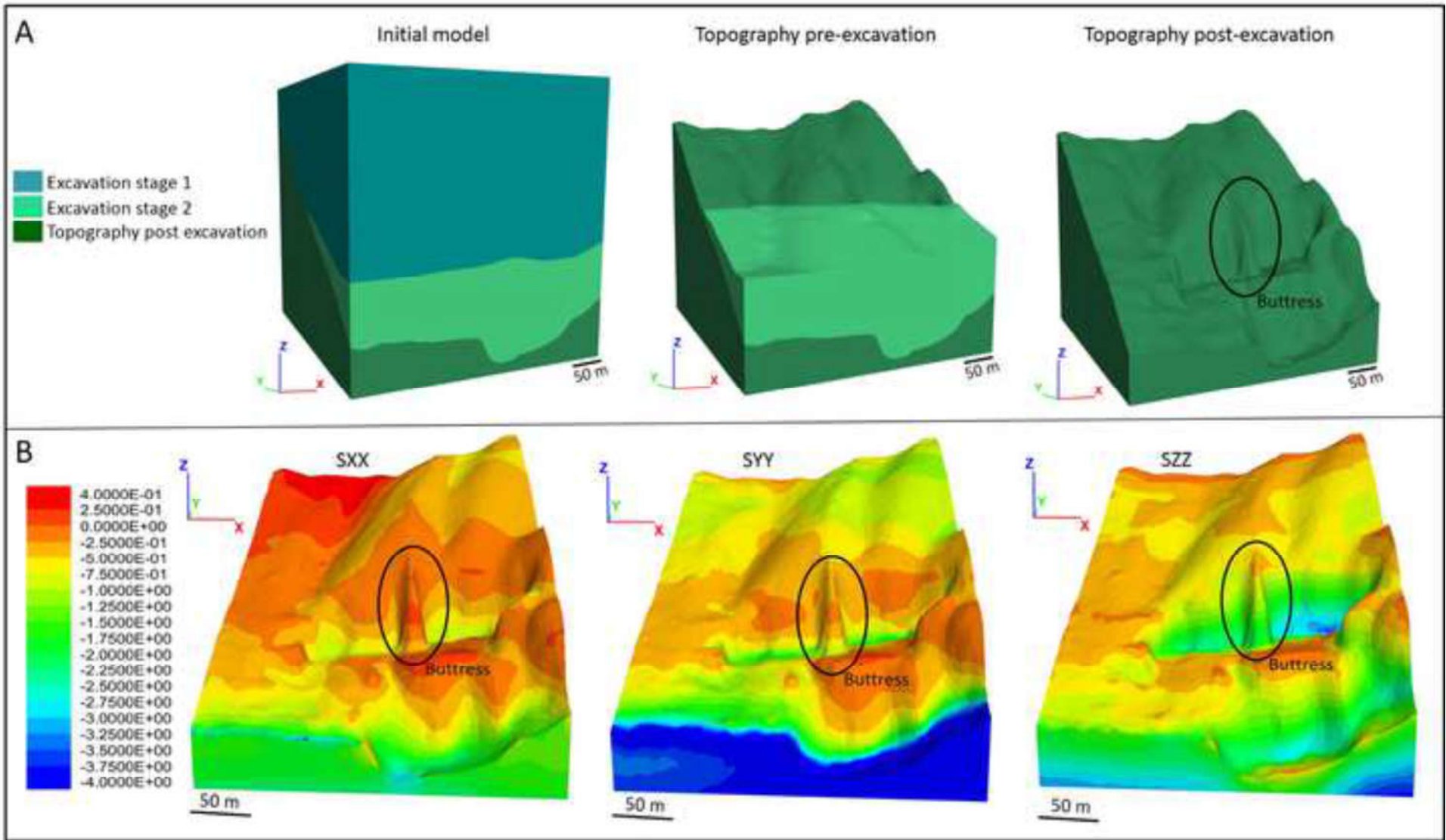
| Kinematic Analysis | Planar Sliding | | |
|----------------------------|-----------------|--------------|----------|
| Slope Dip | 70 | | |
| Slope Dip Direction | 165 | | |
| Friction Angle | 30° | | |
| Lateral Limits | 20° | | |
| | Critical | Total | % |
| Planar Sliding (All) | 16 | 537 | 2.98% |
| Planar Sliding (Set 1: K1) | 12 | 135 | 8.89% |

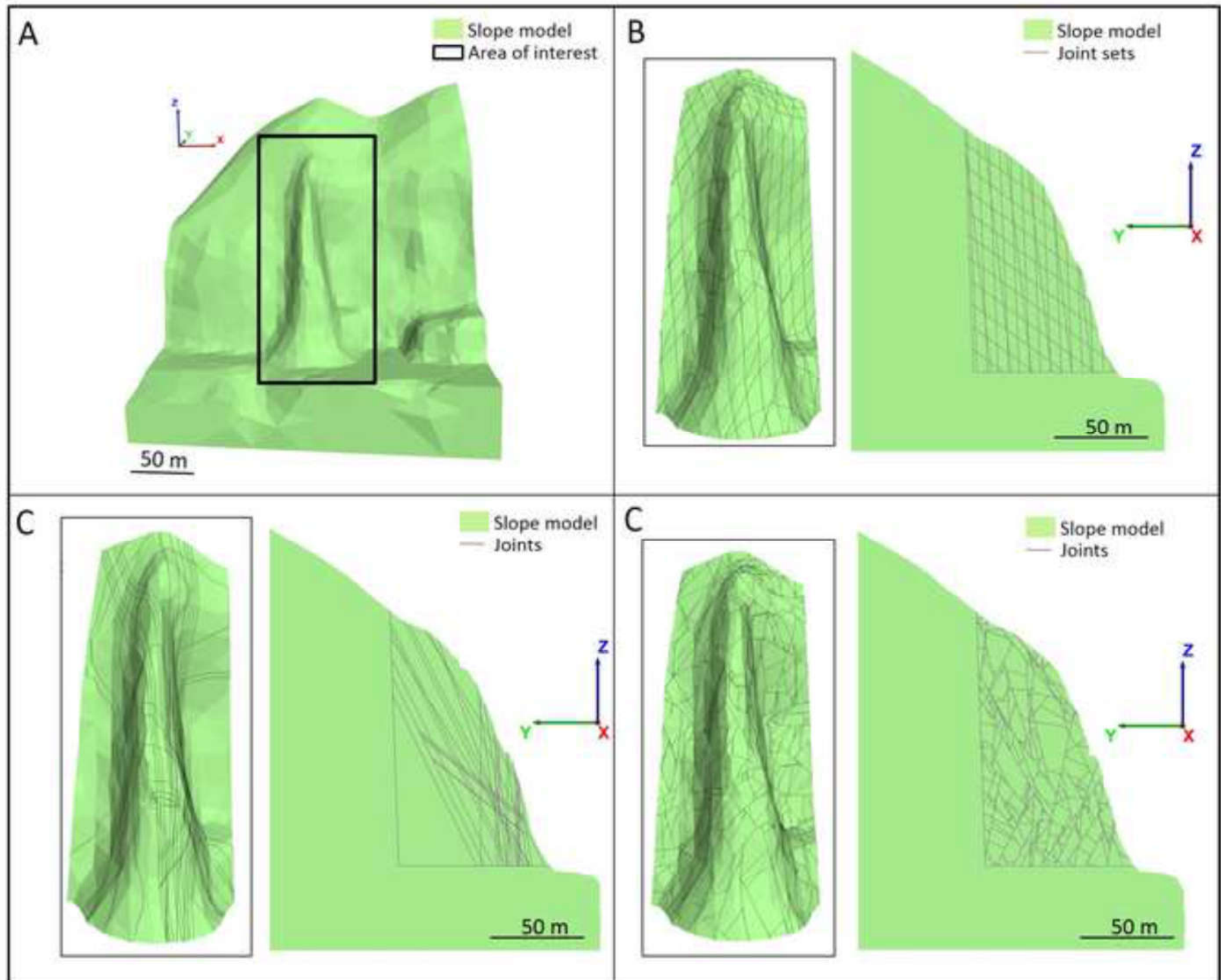


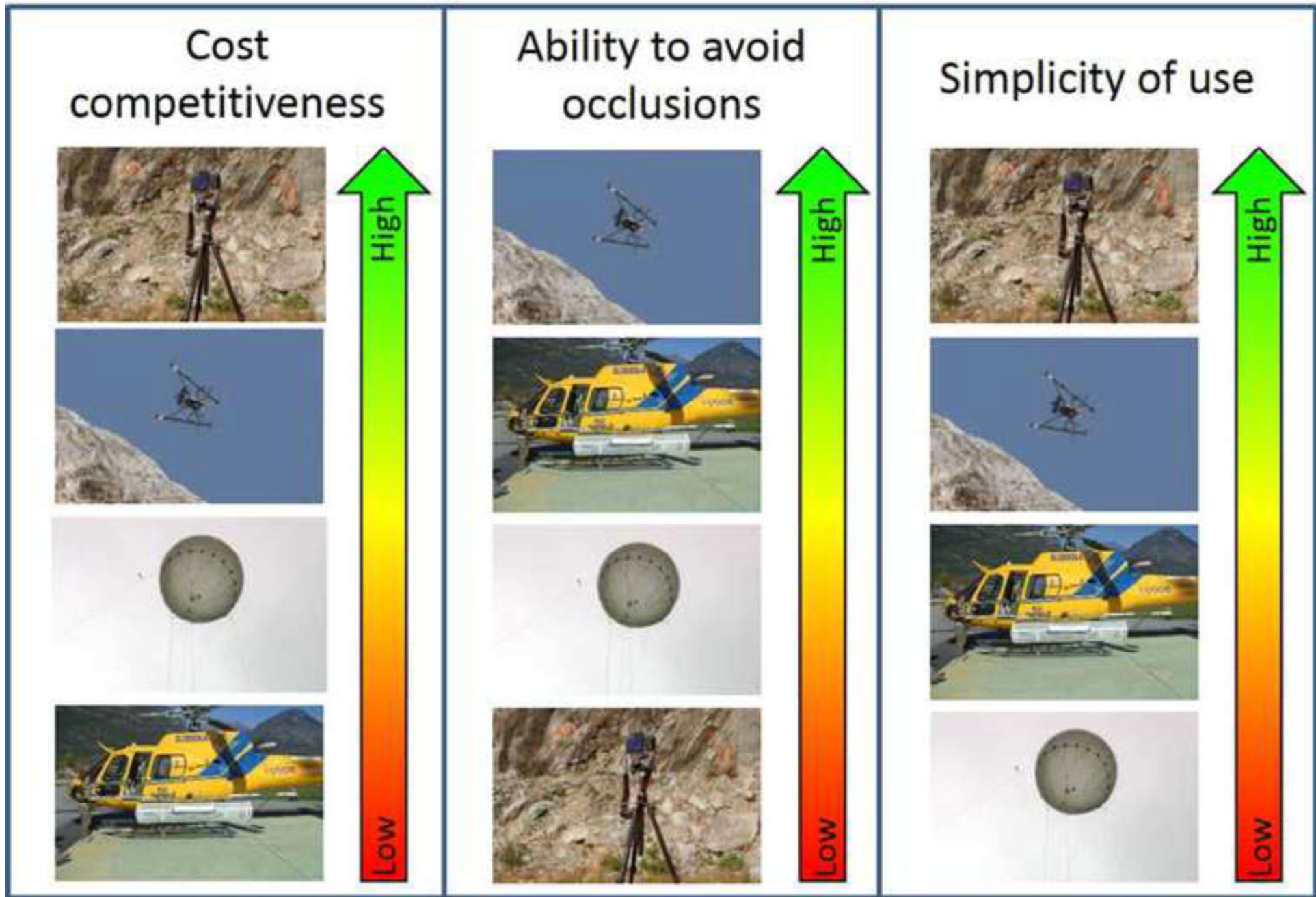












Improvement that geomatic techniques can offer in terms of slope stability analysis input parameters

Type of analyses and possible input parameters

| | | | | |
|--|--------------------|----------------------------|-----------------|--------------------------------------|
| Representative 3D slope geometry is guaranteed even in case of complex geometry. | Kinematic analysis | Limit equilibrium analysis | Runout analysis | More sophisticated numerical methods |
| Geometry and location of joints in rock slopes is known so that to ensure a realistic understanding of wedge formation. Combined with GIS techniques a deterministic or probabilistic kinematic analysis of the slope can be undertaken. | | | | |
| Spatial location of data from remote sensing is representative of the entire slope. | | | | |
| Roughness angles, persistence and spacing can be measured using photogrammetry or LiDAR (Kim et al., 2015 and 2016; Park et al., 2016) and be assigned as discontinuity parameters or attributes to the poles on a stereonet allowing a more insightful kinematic analysis. | | | | |
| Block shape and size can be determined as input for block theory. | | | | |
| Location, shape and volume of every potential unstable block and brittle fracture can be determined making the analysis more realistic and representative. | | | | |
| The presence of eventual loading/support condition and the influence of blasting can be considered. | | | | |
| Accurate slope profile may be derived. | | | | |
| Rear and lateral release as well as failure scars, slope curvature and localized undercut may be defined. | | | | |
| Vegetation and especially roots interacting with potential sliding surface can be located. | | | | |
| Different land covers on the slope can be recognized together with rockfall scars, factors promoting rockfall and evidence of previous failure. Multi-temporal survey (e.g. with DP, LS, LiDAR and Radar Interferometry) can be used for defining debris volume and for change detection (spatial and temporal) analyses (Blasone et al., 2014). | | | | |
| Aerial and terrestrial remote sensing and GIS can be used to detect geomorphic and major structural features and for identifying palaeo-landslides (Clague et al., 2015) and constrain geomechanical models (Sharma et al., 2016). | | | | |
| Heterogeneities can be detected to develop ubiquitous joint rock mass models (Sainsbury et al., 2016). | | | | |
| Thermal images and LS can be used to locate seepage in the slope (Vivas et al., 2013; Gigli et al., 2014). | | | | |
| Thermal and hyperspectral imagery and LS can be used to locate rock weathering and alteration zone (Park et al., 2016). | | | | |
| DFN can be derived and used to understand the role of brittle fracture, persistence, rock bridges, step-paths and connectivity (Elmo, 2006; Tuckey et al., 2013; Hamdi et al., 2015). | | | | |

| DP | Advantages | Limitations |
|-------------------------------------|--|--|
| DP with hand-held camera and tripod | Simple and economic to use. Full control of the camera. In case of tripod, photographs can be acquired with great precision without problems related to vibrations and stability. Wind does not usually affect the survey. | Presence of occlusions in the case of very high slopes. Not possible to use in case of inaccessible areas not facing the object under study. Lighting conditions and distance to outcrop can compromise the survey |
| DP with aerostatic balloon | Overcomes problems related to elevation, steepness and complex geometry of slope. With favourable weather conditions photographs can be acquired with high precision without problems related to the stability of the frame. | Requires experienced user. Maximum elevation of 300 m. Cannot be used where difficult access exists and the slope area is not viewable. Unfavourable weather conditions prevent data acquisition. Use of helium gas is expensive compared to the use of hand-held camera and tripod methods. |
| DP with helicopter | Overcomes problems related to elevation, steepness and complex geometry of slope. Does not need an accessible area facing the slope under study. It is possible to check the photographs acquisition in real time from the helicopter. Differential GPS and IMU control allows calculation of the position and attitude at the moment of the photograph acquisition. Hardware mounted or hand held cameras can be used. | Very expensive in terms of helicopter time requiring careful flight planning. Can be difficult to keep the vehicle stable and in the same direction during data acquisition (this can create major errors during the orientation process; obtaining a large number of photographs and using SfM techniques can reduce these errors). Weather conditions can limit surveys including wind, sun glare on light colour outcrops and restricted visibility due to cloud. |
| DP with UAV | Overcomes problems related to elevation, steepness and complex slope geometry. Does not require the area to face the object under study. Cheap UAV platforms now readily available. Freely available software for data acquisition, flight planning and data processing. | Prone to instability during the photograph acquisition which can result in misalignment of photographs and major error during the orientation process. Acquiring a large number of photographs and using SfM techniques can reduce these errors. Weather conditions can limit the use. Limited battery life requires careful flight planning and may limit application in remote areas. UAV regulations may restrict use or preclude use in some cases. High number of photographs that require processing may necessitate use of high end graphics works station to limit computer run times. |

Table 1. DP platforms: advantages and limitations.

| LS | Advantages | Limitations |
|-----------------|--|--|
| Ground based LS | Simple to use. Slope geometry and geological structure can be rapidly obtained with high precision. | The LS instruments are expensive. Presence of occlusions in the case of very high slopes. Not possible to use in case of inaccessible areas not facing the object under study. |
| Mobile LS | Slope geometry and geological structure can be rapidly derived. Survey of long slope section can be very fast. | The LS instruments are expensive. Presence of occlusions in the case of very high slopes. Precision and accuracy of point cloud can be lower when compared with ground based platforms. Registration of point clouds can be complicated (Michoud et al. 2015). |
| LS with UAV | Slope geometry and geological structure can be rapidly obtained. Overcomes problems related to elevation, steepness and complex slope geometry. Does not need the area to face the object under study. UAV platforms now available. Freely available software for data acquisition, flight planning and data processing. | High cost of LS instruments to be mounted on the UAV. Precision and accuracy of point cloud decrease significantly when compared to ground based platforms. Weather conditions can severely limit use. Limited battery life requires careful flight planning and may limit application in remote areas. UAV regulations may restrict use or preclude use in some cases. |

Table 2. LS platforms: advantages and limitations.